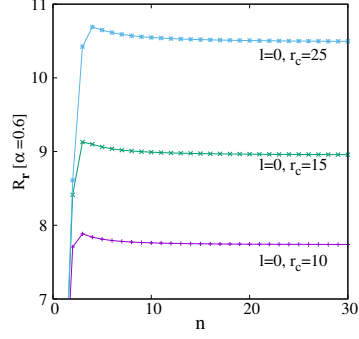


1 Graphical Abstract



Rényi, Shannon, Tsallis entropy, Fisher information and Onicescu energy in conjugate spaces have been reported for a confined Hydrogen atom embedded inside a spherical cavity. The effect of confinement is followed in an arbitrary state. It is found to be more prominent on higher- n states. At small cavity radius, all these measures behave in stark contrast to that found in free Hydrogen atom. Exact analytical results are offered for the circular states in free H atom.

Information-entropic measures in free and confined hydrogen atom

Neetik Mukherjee* and Amlan K. Roy†

Department of Chemical Sciences

Indian Institute of Science Education and Research (IISER) Kolkata,

Mohanpur-741246, Nadia, WB, India

Abstract

Shannon entropy (S), Rényi entropy (R), Tsallis entropy (T), Fisher information (I) and Onicescu energy (E) have been explored extensively in both *free* H atom (FHA) and *confined* H atom (CHA). For a given quantum state, accurate results are presented by employing respective *exact* analytical wave functions in r space. The p -space wave functions are generated from respective Fourier transforms—for FHA these can be expressed analytically in terms of Gegenbauer polynomials, whereas in CHA these are computed numerically. *Exact* mathematical expressions of $R_r^\alpha, R_p^\beta, T_r^\alpha, T_p^\beta, E_r, E_p$ are derived for *circular* states of a FHA. Pilot calculations are done taking order of entropic moments (α, β) as $(\frac{3}{5}, 3)$ in r and p spaces. A detailed, systematic analysis is performed for both FHA and CHA with respect to state indices n, l , and with confinement radius (r_c) for the latter. In a CHA, at small r_c , kinetic energy increases, whereas S_r, R_r^α decrease with growth of n , signifying greater localization in high-lying states. At moderate r_c , there exists an interplay between two mutually opposing factors: (i) radial confinement (localization) and (ii) accumulation of radial nodes with growth of n (delocalization). Most of these results are reported here for the first time, revealing many new interesting features. Comparison with literature results, wherever possible, offers excellent agreement.

PACS: 03.65-w, 03.65Ca, 03.65Ta, 03.65.Ge, 03.67-a.

Keywords: Rényi entropy, Shannon entropy, Fisher information, Tsallis entropy, Onicescu energy, Confined hydrogen atom, Free hydrogen atom.

*Email: neetik.mukherjee@iiserkol.ac.in.

†Corresponding author. Email: akroy@iiserkol.ac.in, akroy6k@gmail.com.

I. INTRODUCTION

A quantum mechanical particle under extreme pressure displays many interesting and notable properties [1–3]. In the last few decades, quantum confinement has emerged as a very fascinating and relevant research area from both theoretical and experimental perspectives [2–7]. Discovery and development of modern experimental techniques have given the required insight about responses of matter under confinement. Furthermore, advancement of nano-science and nano-technology has also stimulated extensive research activity to explore and study such systems. They have potential applications in a wide range of problems in physics and chemistry, namely, quantum wells, quantum wires, quantum dots, defects in solids, super-lattice structure, as well as nano-sized circuits such as quantum computer, etc. Besides, they have uses in cell-model of liquid, high-pressure physics, astrophysics [8], study of impurities in semiconductor materials, matrix isolated molecules, endohedral complexes of fullerenes, zeolites cages, helium droplets, nano-bubbles, [2] etc.

Extensive theoretical works have been published covering a broad variety of confining potentials. Two prototypical systems receiving maximum attention are harmonic oscillator (in 1D, 2D, 3D, D dimension) [9–13] and confined hydrogen atom (CHA) inside a spherical enclosure [3, 14–22]. A CHA within an impenetrable (as well as penetrable) cavity was studied quite vigorously leading to a host of attractive properties—both from physical and mathematical point of view. They offer many unique phenomena, especially relating to *simultaneous, incidental and inter-dimensional* degeneracy [11]. Effect of compression on energy levels of ground and excited states, as well as other properties like hyperfine splitting constant, dipole shielding factor, nuclear magnetic screening constant, pressure, static and dynamic polarizability, etc., were examined [2, 3, 23]. Numerous theoretical methods varying in complexity, sophistication were employed; a selected set includes perturbation theory, Padé approximation, WKB method, Hypervirial theorem, power-series solution, super-symmetric quantum mechanics, Lie algebra, Lagrange-mesh method, asymptotic iteration method, generalized pseudo-spectral method, etc. [14–22] and references therein. *Exact* solutions [18] are expressible in terms of Kummer M-function (confluent hypergeometric).

In recent years, appreciable attention was paid to investigate various information measures, namely, Fisher information (I), Shannon entropy (S), Rényi entropy (R), Tsallis entropy (T), Onicescu energy (E) and several complexities in a multitude of physical and

chemical systems including central potentials. The literature is quite vast. Here we restrict ourselves to a few references pertaining to H atom. Some of these for an unconfined *free* H atom (FHA) are: I_r, I_p, I in 3D [24], in D-dimension [25–27], upper bounds of S, R [28], S in 3D [29], in D-dimension [30], R, T in 3D [29], in D-dimension [31]. Relativistic effects on the information measures of FHA are also examined [32]. A lucid review on information theory of D-dimensional FHA is provided in [33]. However, in CHA such studies are quite scarce, *viz.*, S [34, 35], bounds of I, S, R, T [36], I, S in case of soft spherically CHA [37].

In a quantum system, S and I quantify the information content in different and complementary way. Former refers to the expectation value of logarithmic probability density function and is a global measure of spread of density. On the other hand, I is a gradient functional of density and in position (r) space, it quantifies the oscillatory nature and narrowness of density. In recent years, S is examined in a number of occasions, such as, Pöschl-Teller [38], Rosen-Morse [39], pseudo-harmonic [40], squared tangent well [41], hyperbolic [42], position-dependent mass Schrödinger equation [43, 44], infinite circular well [45], hyperbolic double-well (DW) potential [46], etc. In parallel, I is found to be a useful tool to analyze various atomic and molecular systems [47–49]. Analytical expressions for I are obtained for generalized central potentials in both r and momentum (p) space [24]. E is quantified as the second-order entropic moment [50]. It becomes minimum for equilibrium and hence often termed as disequilibrium. Recently, some of these measures have been found to be quite effective and useful to explain the oscillation and localization-delocalization behavior of a particle in symmetric and asymmetric DW potential [51, 52], as well as in a confined 1D quantum harmonic oscillator [13].

It is well known that, R^α, T^α , the so-called information generating functionals, are closely connected to entropic moments (discussed later), and completely characterize density $\rho(\mathbf{r})$. They are expressed in terms of expectation values of density, in following conventional forms,

$$\begin{aligned} R^\alpha[\rho(\mathbf{r})] &= \frac{1}{(1-\alpha)} \ln \langle \rho(\mathbf{r})^{(\alpha-1)} \rangle, \\ T^\alpha[\rho(\mathbf{r})] &= \frac{1}{(\alpha-1)} [1 - \langle \rho(\mathbf{r})^{(\alpha-1)} \rangle] \quad 0 < \alpha < \infty, \quad \alpha \neq 1. \end{aligned} \tag{1}$$

Untitled Folder They actually quantify the spatial delocalization of single-particle density of a system in various complementary ways. Arguably, these are the most appropriate uncertainty measures, as they do not make any reference to some specific point of the corresponding Hilbert space. Moreover, these are closely related to energetic and experimentally

measurable quantities [23, 53] of a system. In case of R and S , some lower bound is available, which does not depend on quantum number. But, for I both upper and lower bounds have been established, which strictly change with quantum numbers [24, 54, 55].

It is interesting to note that, S , E (disequilibrium) are two particular cases of R^α, T^α [23, 54]. Former measures total extent of density whereas E quantifies separation of density with respect to equilibrium. They are related to R^α, T^α in following way [31],

$$\begin{aligned} S[\rho] &= - \int \rho(\mathbf{r}) \ln \rho(\mathbf{r}) d\mathbf{r} = \lim_{\alpha \rightarrow 1} R^\alpha[\rho] = \lim_{\alpha \rightarrow 1} T^\alpha[\rho], \\ E &= \langle \rho \rangle = \exp(R^2[\rho]), \quad \langle \rho \rangle = \int \rho^2(\mathbf{r}) d\mathbf{r}. \end{aligned} \quad (2)$$

Lately, Rényi entropy has been successfully employed to investigate and predict various quantum properties and phenomena like entanglement, communication protocol, correlation de-coherence, measurement, localization properties of Rydberg states, molecular reactivity, multi-fractal thermodynamics, production of multi-particle in high-energy collision, disordered systems, spin system, quantum-classical correspondence, localization in phase space [56–62], etc. Likewise, T has been also been studied, albeit with rather lesser intensity. It has been implicated for non-extensive thermo-statistics [63, 64] and exploited quite extensively in the field of image processing, power-signal analysis, gravitation [65, 66], etc.

These information measure may be used in FHA, CHA to understand diffused nature of orbitals. All these are statistical quantities and are directly related to single-particle density. Also, results of one quantity compliments the inferences of others. In FHA, they help to grasp the spreading of orbitals at higher states. Whereas, in CHA, R, T, S, E qualitatively explain the effect of confinement on an arbitrary n, l, m state. As found in later section, with increase in R_r, T_r, S_r and decrease in E_r , system gets delocalized and vice versa.

The present communication has several objectives. Our primary motivation is to undertake a detailed analysis of S, I, R, T, E in a FHA in a systematic fashion for an arbitrary state in both spaces. To put things in proper perspective, it is worth mentioning the scattered results that are available in literature for a FHA. The *exact* mathematical form of I for an *arbitrary* state of FHA was given in both r and p space [24] in terms of four expectation values $\langle r^2 \rangle, \langle r^{-2} \rangle, \langle p^2 \rangle, \langle p^{-2} \rangle$, and eventually in terms of the related quantum numbers. Likewise, an *exact* analytical formula for S in *ground state* of a D-dimensional FHA was derived long times ago [30] in both r and p space. Later, similar analytical expressions of S for *circular or node-less* states of a D-dimensional FHA was offered in 2010 [33] in both

spaces. However, such a closed-form expression of S is as yet lacking for a *general* state. Very recently, in [35], accurate radial Shannon entropies in r, p spaces with $n \leq 10$ are computed numerically. Moreover, a generalized form of angular shannon entropy was also derived. Recently, R and T were studied for Rydberg hydrogenic states within a strong Laguerre asymptotic approximation [29, 31]. But, their *exact* solutions are as yet unknown; moreover these were reported only in r space and mostly for $l = 0$ states. And to the best of our knowledge, E has not yet been explored at all whatsoever. Thus there is some gap in the understanding of information-entropic measures in this system. This work makes an attempt to fill this void and embarks on an elaborate analysis of all these quantities in *both* spaces for a *general* state having principal and azimuthal quantum numbers n, l , while keeping magnetic quantum number $m = 0$. For free system, all these can be calculated from *exact* analytical wave functions in r, p space. It is found that, for node-less states, expressions of S, R, T, E are accessible in closed form in a FHA, as the required radial polynomial reduces to unity. But for all other, n, l , they need to be computed numerically, as presence of nodes in such wave functions leads to difficult polynomials. Next, we proceed for a parallel analysis for a CHA at varying r_c , taking *exact* wave function in r space. However such expressions are unavailable in p space, and hence numerical Fourier transforms need to be carried out. Unlike the case of FHA, all measures in a CHA have to be obtained numerically—in both r, p spaces. Note that such studies in CHA are very rare. Apart from the work of [35] for S (as mentioned above), it was studied in the context of soft and hard confinement in lowest state [34, 37]. Further in [35], variation of S in s, p, d orbitals ($n \leq 7$) was followed with r_c . Thus it is very desirable to probe these with respect to state indices and r_c . Throughout the article, comparison with existing literature results are made wherever possible. Organization of our article is as follows. Section II gives essential components of methodology; then Sec. III gives a detailed discussion on the results of above-mentioned quantities for FHA and CHA, while we conclude with a few remarks in Sec. IV.

II. METHODOLOGY

Without any loss of generality, the time-independent non-relativistic wave function for a hydrogenic system, in r space can be written as ($\mathbf{r} = \{r, \Omega\}$),

$$\Psi_{n,l,m}(\mathbf{r}) = \psi_{n,l}(r) Y_{l,m}(\Omega), \quad (3)$$

TABLE I: The co-efficients a_k and b_j for even- l p -space wave functions in FHA. See text for details.

l	b_0	b_2	b_4	b_6	b_8	a_1	a_3	a_5	a_7
0	$\frac{1}{\sqrt{\pi}}$	—	—	—	—	—	—	—	—
2	$\frac{1}{\sqrt{\pi}}$	$-\frac{3}{\sqrt{\pi}}$	—	—	—	$\frac{3}{\sqrt{\pi}}$	—	—	—
4	$\frac{1}{\sqrt{\pi}}$	$-\frac{105}{\sqrt{\pi}}$	$\frac{315}{\sqrt{\pi}}$	—	—	$\frac{30}{\sqrt{\pi}}$	$-\frac{315}{\sqrt{\pi}}$	—	—
6	$\frac{1}{\sqrt{\pi}}$	$-\frac{210}{\sqrt{\pi}}$	$\frac{4725}{\sqrt{\pi}}$	$-\frac{10395}{\sqrt{\pi}}$	—	$\frac{21}{\sqrt{\pi}}$	$-\frac{1260}{\sqrt{\pi}}$	$\frac{10395}{\sqrt{\pi}}$	—
8	$\frac{1}{\sqrt{\pi}}$	$-\frac{630}{\sqrt{\pi}}$	$\frac{51975}{\sqrt{\pi}}$	$-\frac{945945}{\sqrt{\pi}}$	$\frac{2027025}{\sqrt{\pi}}$	$\frac{36}{\sqrt{\pi}}$	$-\frac{6930}{\sqrt{\pi}}$	$\frac{270270}{\sqrt{\pi}}$	$-\frac{2027025}{\sqrt{\pi}}$

with r and Ω denoting radial distance and solid angle respectively. Here $\psi_{n,l}(r)$ corresponds to radial part and $Y_{l,m}(\Omega)$ the spherical harmonics of atomic state, determined by quantum numbers (n, l, m) . In what follows, atomic units employed unless otherwise mentioned and \mathbf{r}, \mathbf{p} subscripts denote quantities in full r and p spaces (including angular part) respectively.

The relevant radial Schrödinger equation under the influence of confinement is,

$$\left[-\frac{1}{2} \frac{d^2}{dr^2} + \frac{l(l+1)}{2r^2} + v(r) + v_c(r) \right] \psi_{n,l}(r) = \mathcal{E}_{n,l} \psi_{n,l}(r), \quad (4)$$

where $v(r) = -Z/r$ ($Z = 1$ for H atom). Our desired confinement inside an impenetrable spherical cage is accomplished by invoking the following potential: $v_c(r) = +\infty$ for $r > r_c$, and 0 for $r \leq r_c$, where r_c signifies radius of the box. This equation needs to be solved under Dirichlet boundary condition, $\psi_{n,l}(0) = \psi_{n,l}(r_c) = 0$.

Angular part has following common form in both r and p spaces ($P_l^m(\cos \theta)$ signifies usual associated Legendre polynomial),

$$Y_{l,m}(\Omega) = \Theta_{l,m}(\theta) \Phi_m(\phi) = (-1)^m \sqrt{\frac{2l+1}{4\pi} \frac{(l-m)!}{(l+m)!}} P_l^m(\cos \theta) e^{-im\phi}. \quad (5)$$

The exact generalized radial wave function for a CHA can be expressed [18] as,

$$\psi_{n,l}(r) = N_{n,l} \left(2r \sqrt{-2\mathcal{E}_{n,l}} \right)^l {}_1F_1 \left[\left(l+1 - \frac{1}{\sqrt{-2\mathcal{E}_{n,l}}} \right), (2l+2), 2r \sqrt{-2\mathcal{E}_{n,l}} \right] e^{-r \sqrt{-2\mathcal{E}_{n,l}}}, \quad (6)$$

where $N_{n,l}$ denotes normalization constant and $\mathcal{E}_{n,l}$ corresponds to energy of a given state characterized by n, l quantum numbers, whereas ${}_1F_1[a, b, r]$ represents confluent hypergeometric function. In case of FHA ($r_c \rightarrow \infty$), the first-order hypergeometric function reduces to associated Laguerre polynomial with $\mathcal{E}_{n,l} = -\frac{Z^2}{2n^2}$ (Z denotes atomic number); so the radial function simplifies to commonly used form, as given below,

$$\psi_{n,l}(r) = \frac{2}{n^2} \left[\frac{(n-l-1)!}{(n+l)!} \right]^{\frac{1}{2}} \left[\frac{2Z}{n} r \right]^l e^{-\frac{Z}{n}r} L_{(n-l-1)}^{(2l+1)} \left(\frac{2Z}{n} r \right). \quad (7)$$

TABLE II: The co-efficients a_k and b_j for odd- l p -space wave functions in FHA. See text for details.

l	a_0	a_2	a_4	a_6	a_8	b_1	b_3	b_5	b_7	b_9
1	$\frac{1}{\sqrt{\pi}}$	—	—	—	—	$-\frac{1}{\sqrt{\pi}}$	—	—	—	—
3	$\frac{1}{\sqrt{\pi}}$	$-\frac{15}{\sqrt{\pi}}$	—	—	—	$-\frac{3!}{\sqrt{\pi}}$	$\frac{15}{\sqrt{\pi}}$	—	—	—
5	$\frac{1}{\sqrt{\pi}}$	$-\frac{105}{\sqrt{\pi}}$	$\frac{945}{\sqrt{\pi}}$	—	—	$-\frac{15}{\sqrt{\pi}}$	$\frac{420}{\sqrt{\pi}}$	$-\frac{945}{\sqrt{\pi}}$	—	—
7	$\frac{1}{\sqrt{\pi}}$	$-\frac{378}{\sqrt{\pi}}$	$\frac{17325}{\sqrt{\pi}}$	$-\frac{135135}{\sqrt{\pi}}$	—	$-\frac{28}{\sqrt{\pi}}$	$\frac{3150}{\sqrt{\pi}}$	$-\frac{2370}{\sqrt{\pi}}$	$\frac{135135}{\sqrt{\pi}}$	—
9	$\frac{1}{\sqrt{\pi}}$	$-\frac{990}{\sqrt{\pi}}$	$\frac{135135}{\sqrt{\pi}}$	$-\frac{4729725}{\sqrt{\pi}}$	$\frac{34459425}{\sqrt{\pi}}$	$-\frac{45}{\sqrt{\pi}}$	$\frac{13860}{\sqrt{\pi}}$	$-\frac{945945}{\sqrt{\pi}}$	$\frac{16216200}{\sqrt{\pi}}$	$-\frac{34459425}{\sqrt{\pi}}$

Thus allowed energies at a specific r_c can be obtained by finding the zeros of ${}_1F_1$,

$${}_1F_1 \left[\left(l + 1 - \frac{1}{\sqrt{-2\mathcal{E}_{n,l}}} \right), (2l + 2), 2r_c \sqrt{-2\mathcal{E}_{n,l}} \right] = 0. \quad (8)$$

For a particular l , first root corresponds to energy of the lowest- n state ($n_{lowest} = l + 1$) with successive roots identifying excited states. It is instructive to note that, in order to construct the exact wave function of CHA for a specific state, one needs to supply energy eigenvalue of that state. In our present calculation, $\mathcal{E}_{n,l}$ of CHA, computed by means of the generalized pseudo-spectral (GPS) method is employed, because for a number of central potentials as in current situation, this has produced highly accurate eigenvalues and eigenfunctions, in both free and confinement situations; see e.g., references [12, 22, 67–69] and therein for some of the developments. Note that in this communication, our objective is not precise calculation of energy; rather we are interested in the information measures in CHA, for which GPS energies are sufficiently accurate to obtain correct eigenfunctions.

The p -space wave function ($\mathbf{p} = \{p, \Omega\}$) for a particle in a central potential is obtained from respective Fourier transform of its r -space counterpart, and as such, is given below,

$$\begin{aligned} \psi_{n,l}(p) &= \frac{1}{(2\pi)^{\frac{3}{2}}} \int_0^\infty \int_0^\pi \int_0^{2\pi} \psi_{n,l}(r) \Theta(\theta) \Phi(\phi) e^{ipr \cos \theta} r^2 \sin \theta \, dr d\theta d\phi, \\ &= \frac{1}{2\pi} \sqrt{\frac{2l+1}{2}} \int_0^\infty \int_0^\pi \psi_{n,l}(r) P_l^0(\cos \theta) e^{ipr \cos \theta} r^2 \sin \theta \, dr d\theta. \end{aligned} \quad (9)$$

Note that $\psi(p)$ is not normalized; thus needs to be normalized. Integrating over θ and ϕ variables, Eq. (9) can be further reduced to,

$$\psi_{n,l}(p) = (-i)^l \int_0^\infty \frac{\psi_{n,l}(r)}{p} f(r, p) dr. \quad (10)$$

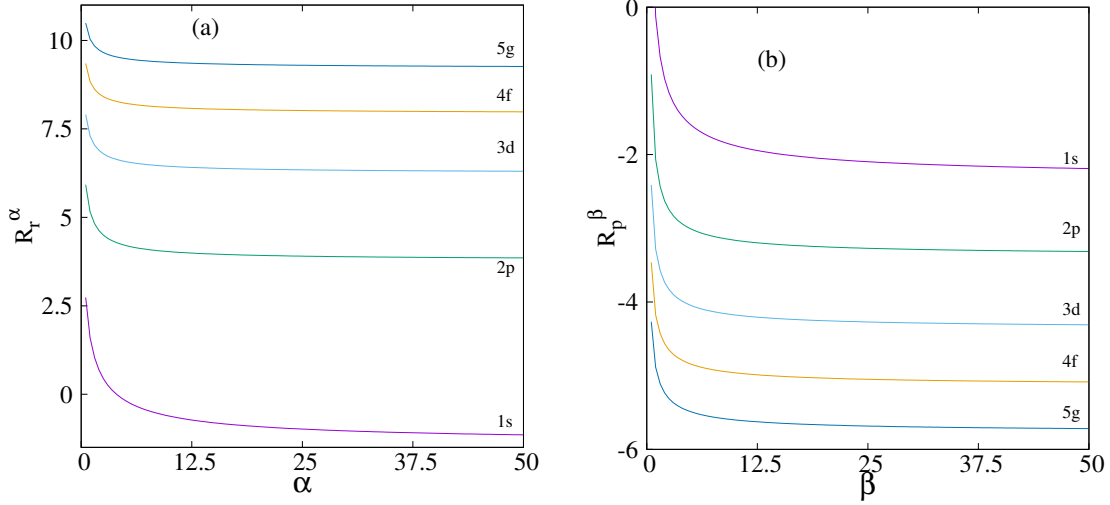


FIG. 1: Variation of R_r^α and R_p^β with respect to α and β for $1s$, $2p$, $3d$, $4f$, $5g$ states of FHA, in panels (a), (b) respectively. More details can be found in the text.

Depending on l , this can be rewritten in following simplified form (m' starts with 0),

$$\begin{aligned}
 f(r, p) &= \sum_{k=2m'+1}^{m' < \frac{l}{2}} a_k \frac{\cos pr}{p^k r^{k-1}} + \sum_{j=2m'}^{m' = \frac{l}{2}} b_j \frac{\sin pr}{p^j r^{j-1}}, \quad \text{for even } l, \\
 f(r, p) &= \sum_{k=2m'}^{m' = \frac{l-1}{2}} a_k \frac{\cos pr}{p^k r^{k-1}} + \sum_{j=2m'+1}^{m' = \frac{l-1}{2}} b_j \frac{\sin pr}{p^j r^{j-1}}, \quad \text{for odd } l.
 \end{aligned} \tag{11}$$

The coefficients a_k , b_j of even- l and odd- l states are collected in Tables I and II respectively.

For a FHA, one can achieve the following analytical expression for wave function [70],

$$\psi_{n,l}(p) = n^2 \left[\frac{2}{\pi} \frac{(n-l-1)!}{(n+l)!} \right]^{\frac{1}{2}} 2^{(2l+2)} l! \frac{n^l}{\left\{ \left[\frac{np}{Z} \right]^2 + 1 \right\}^{l+2}} \left(\frac{p}{Z} \right)^l C_{n-l-1}^{l+1} \left(\frac{\left[\frac{np}{Z} \right]^2 - 1}{\left[\frac{np}{Z} \right]^2 + 1} \right), \tag{12}$$

where $C_\zeta^\eta(t)$ signifies the Gegenbauer polynomial.

It is known that $I_{\mathbf{r}}$, $I_{\mathbf{p}}$ for a single particle in a central potential can be written in terms of radial expectation values $\langle r^k \rangle$ and $\langle p^k \rangle$, ($k = -2, 2$) [24],

$$\begin{aligned}
 I_{\mathbf{r}} &= \int_{\mathcal{R}^3} \left[\frac{|\nabla \rho(\mathbf{r})|^2}{\rho(\mathbf{r})} \right] d\mathbf{r} = 4\langle p^2 \rangle - 2(2l+1)|m|\langle r^{-2} \rangle; \quad \rho(\mathbf{r}) = |\psi_{n,l,m}(\mathbf{r})|^2, \\
 I_{\mathbf{p}} &= \int_{\mathcal{R}^3} \left[\frac{|\nabla \Pi(\mathbf{p})|^2}{\Pi(\mathbf{p})} \right] d\mathbf{p} = 4\langle r^2 \rangle - 2(2l+1)|m|\langle p^{-2} \rangle; \quad \Pi(\mathbf{p}) = |\psi_{n,l,m}(\mathbf{p})|^2.
 \end{aligned} \tag{13}$$

Whereas the **total position-momentum (PM) Fisher information** is expressed as, $I = I_{\mathbf{r}} I_{\mathbf{p}}$.

It satisfies the following bound [24],

$$\frac{81}{\langle r^2 \rangle \langle p^2 \rangle} \leq I_{\mathbf{r}} I_{\mathbf{p}} \leq 16 \langle r^2 \rangle \langle p^2 \rangle. \tag{14}$$

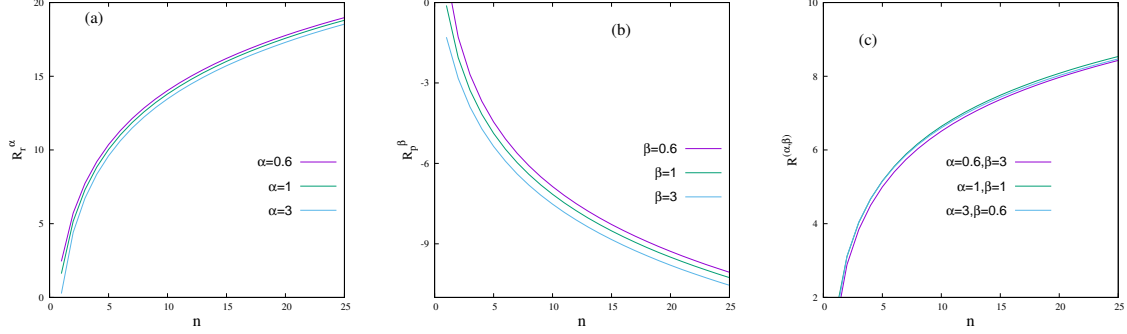


FIG. 2: Plots of R_r^α , R_p^β , **radial PM Rényi entropy** $R^{(\alpha,\beta)}$ against n for some circular states of FHA at three specific sets of α, β , (α, β) values, in panels (a), (b), (c) respectively. See text for details.

Here $\rho(\mathbf{r})$, $\Pi(\mathbf{p})$ signify r - and p -space densities, both being normalized to unity. Next, S_r , S_p and **total PM Shannon entropy** S is defined in terms of expectation values of logarithmic probability density functions, which for a central potential further simplifies [55] as below,

$$S_r = - \int_{\mathcal{R}^3} \rho(\mathbf{r}) \ln[\rho(\mathbf{r})] d\mathbf{r} = 2\pi (S_r + S_{(\theta,\phi)}), S_p = - \int_{\mathcal{R}^3} \Pi(\mathbf{p}) \ln[\Pi(\mathbf{p})] d\mathbf{p} = 2\pi (S_p + S_{(\theta,\phi)}),$$

$$S = 2\pi [S_r + S_p + 2S_{(\theta,\phi)}] \geq 3(1 + \ln \pi), \quad (15)$$

where the quantities S_r , S_p and S_θ are defined as [55],

$$S_r = - \int_0^\infty \rho(r) \ln[\rho(r)] r^2 dr, \quad S_p = - \int_0^\infty \Pi(p) \ln[\Pi(p)] p^2 dp,$$

$$\rho(r) = |\psi_{n,l}(r)|^2, \quad \Pi(p) = |\psi_{n,l}(p)|^2, \quad (16)$$

$$S_{(\theta,\phi)} = - \int_0^\pi \chi(\theta) \ln[\chi(\theta)] \sin \theta d\theta, \quad \chi(\theta) = |\Theta(\theta)|^2.$$

Similarly, Rényi entropies of order $\lambda (\neq 1)$ are obtained by taking logarithm of λ -order entropic moment. In spherical polar coordinate these can be written in following simplified form by some straightforward mathematical manipulation,

$$R_r^\lambda = \frac{1}{1-\lambda} \ln \left(\int_{\mathcal{R}^3} \rho^\lambda(\mathbf{r}) d\mathbf{r} \right) = \frac{1}{(1-\lambda)} \ln \left(2\pi \int_0^\infty [\rho(r)]^\lambda r^2 dr \int_0^\pi [\chi(\theta)]^\lambda \sin \theta d\theta \right)$$

$$= \frac{1}{(1-\lambda)} (\ln 2\pi + \ln[\omega_r^\lambda] + \ln[\omega_{(\theta,\phi)}^\lambda]),$$

$$R_p^\lambda = \frac{1}{1-\lambda} \ln \left[\int_{\mathcal{R}^3} \Pi^\lambda(\mathbf{p}) d\mathbf{p} \right] = \frac{1}{(1-\lambda)} \ln \left(2\pi \int_0^\infty [\Pi(p)]^\lambda p^2 dp \int_0^\pi [\chi(\theta)]^\lambda \sin \theta d\theta \right) \quad (17)$$

$$= \frac{1}{(1-\lambda)} (\ln 2\pi + \ln[\omega_p^\lambda] + \ln[\omega_{(\theta,\phi)}^\lambda]).$$

TABLE III: Angular contributions, $S_{(\theta,\phi)}$, $R_{(\theta,\phi)}^\alpha$, $R_{(\theta,\phi)}^\beta$, $T_{(\theta,\phi)}^\alpha$, $T_{(\theta,\phi)}^\beta$, $E_{(\theta,\phi)}$ in H atom ($m = 0$), for the selected value of $\alpha = \frac{3}{5}, \beta = 3$ for 10 lowest l states. More details are available in text.

l	$S_{(\theta,\phi)}^\P$	$R_{(\theta,\phi)}^\alpha$	$R_{(\theta,\phi)}^\beta$	$T_{(\theta,\phi)}^\alpha$	$T_{(\theta,\phi)}^\beta$	$E_{(\theta,\phi)}$
0	2.531024246969	2.531024246969	2.531024246969	4.380562660576	0.4968337130111	0.0795774715459
1	2.0990786249678	2.207799279060	1.856060888495	3.546081906570	0.4877871787573	0.1432394487826
2	2.0411250061339	2.1880740866193	1.586098811200	3.498565470109	0.4790443043946	0.17052315331268
3	2.0206596227683	2.1838712989476	1.4135979721010	3.488489128929	0.4704107193889	0.18775831398309
4	2.0105368074094	2.1825847862425	1.2861478982321	3.485418316773	0.4618199815337	0.20037698056464
5	2.0045776990712	2.1821358741265	1.1848960592462	3.484336298921	0.4532499193936	0.21034302374067
6	2.0006768495387	2.1819848295620	1.1008390899096	3.483972643154	0.4446913166609	0.21858446105644
7	1.997934606130	2.1819528334935	1.028955122477	3.483896265386	0.4361397020166	0.22561345675926
8	1.9959057777584	2.1819710153868	0.96615017473812	3.483938671551	0.4275926546791	0.23174282746972
9	1.9943460712042	2.1820101260317	0.91038050803346	3.484031759027	0.4190487531790	0.23717779214936

^{\P}Literature results [35] of $S_{(\theta,\phi)}$ for $l = 0 - 9$ and $m = 0$ states are: 2.5310242469692, 2.0990786249678, 2.0411250061339, 2.0206596227683, 2.0105368074095, 2.0045776990714, 2.0006768495387, 1.9979346061302, 1.9959057777583, 1.9943460712038 respectively.

Here ω_r^λ s are entropic moments in τ (r or p or θ) space with order λ , having forms,

$$\omega_r^\lambda = \int_0^\infty [\rho(r)]^\lambda r^2 dr, \quad \omega_p^\lambda = \int_0^\infty [\Pi(p)]^\lambda p^2 dp, \quad \omega_{(\theta,\phi)}^\lambda = \int_0^\pi [\chi(\theta)]^\lambda \sin \theta d\theta. \quad (18)$$

If λ corresponds to α, β in r, p spaces respectively, then for Rényi and Tsallis entropies, they obey the condition $\frac{1}{\alpha} + \frac{1}{\beta} = 2$. Then one can define **total PM Rényi entropy** as $R^{(\alpha,\beta)}$ [23, 54],

$$\begin{aligned} R^{(\alpha,\beta)} &= \frac{2 - \alpha - \beta}{(1 - \alpha)(1 - \beta)} \ln 2\pi + \frac{1}{(1 - \alpha)} (\ln[\omega_r^\alpha] + \ln[\omega_{(\theta,\phi)}^\alpha]) + \frac{1}{(1 - \beta)} (\ln[\omega_p^\beta] + \ln[\omega_{(\theta,\phi)}^\beta]) \\ &\geq 3 \times \left[-\frac{1}{2} \left(\frac{\ln \alpha}{1 - \alpha} + \frac{\ln \beta}{1 - \beta} \right) - \ln \left(\frac{\Delta r \Delta p}{\hbar \pi} \right) \right]. \end{aligned} \quad (19)$$

Δr and Δp are standard deviation in position and momentum space respectively.

Finally, Tsallis entropy [71] in r, p spaces are expressed as below,

$$\begin{aligned} T_{\mathbf{r}}^\alpha &= \left(\frac{1}{\alpha - 1} \right) \left[1 - \int_{\mathcal{R}^3} \rho^\alpha(\mathbf{r}) d\mathbf{r} \right] = \left(\frac{1}{\alpha - 1} \right) [1 - 2\pi \omega_r^\alpha \omega_{(\theta,\phi)}^\alpha], \\ T_{\mathbf{p}}^\beta &= \left(\frac{1}{\beta - 1} \right) \left[1 - \int_{\mathcal{R}^3} \Pi^\beta(\mathbf{p}) d\mathbf{p} \right] = \left(\frac{1}{\beta - 1} \right) [1 - 2\pi \omega_r^\beta \omega_{(\theta,\phi)}^\beta]. \end{aligned} \quad (20)$$

The corresponding **total PM Tsallis entropy** is then given by, $T^{(\alpha,\beta)} = T_{\mathbf{r}}^\alpha T_{\mathbf{p}}^\beta$.

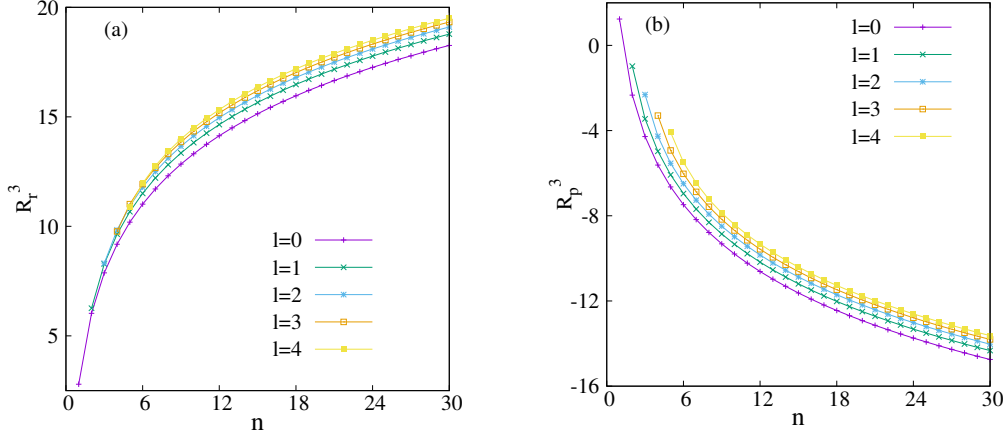


FIG. 3: Variation of R_r^α, R_p^β with n , for lowest five l (0-4) states, in panels (a)-(b), in a FHA. Both α, β are chosen as 3. For more details, consult text.

By definition, E refers to the 2nd order entropic moment [23]; therefore choice of $\alpha = \beta = 2$ transforms Eq. (18) into the form,

$$E_r = \int_0^\infty [\rho(r)]^2 r^2 dr, \quad E_p = \int_0^\infty [\Pi(p)]^2 p^2 dp, \quad E_{\theta, \phi} = \int_0^\pi [\chi(\theta)]^2 \sin \theta d\theta, \quad E = E_r E_p E_{\theta, \phi}^2. \quad (21)$$

where, E is the total PM Onicescu energy. Note that, the restriction $\frac{1}{\alpha} + \frac{1}{\beta} = 2$ holds for R and T only, and not E . Hence in our study of R, T , $\alpha = \frac{3}{5}$ and $\beta = 3$ have been chosen.

III. RESULT AND DISCUSSION

For ease of presentation, it would be appropriate to mention a few things at the outset. The *net* information measures in r and p space of FHA and CHA may be branched into two separate contributions, *viz.*, (i) a radial and (ii) an angular part. It is clear from Eqs. (6) and (7) that, general form of radial wave function changes from CHA to FHA. As mentioned earlier, except the p space of CHA, radial wave functions are available in closed analytical forms, in r and p spaces, both for FHA and CHA; and hence employed throughout all tables and figures in this section. As discussed later, it follows that in case of FHA, one can derive analytical expressions for all these quantities, for the special case of *node-less* ($n - l = 1$) states. Note that, angular portion of these measures remains invariant in r, p spaces in both systems, and they also will not change with respect to boundary condition in r_c in a CHA. Furthermore, they change with l, m quantum numbers. In present calculation, we have chosen magnetic quantum number m as 0, unless stated otherwise. Lastly, in case of FHA,

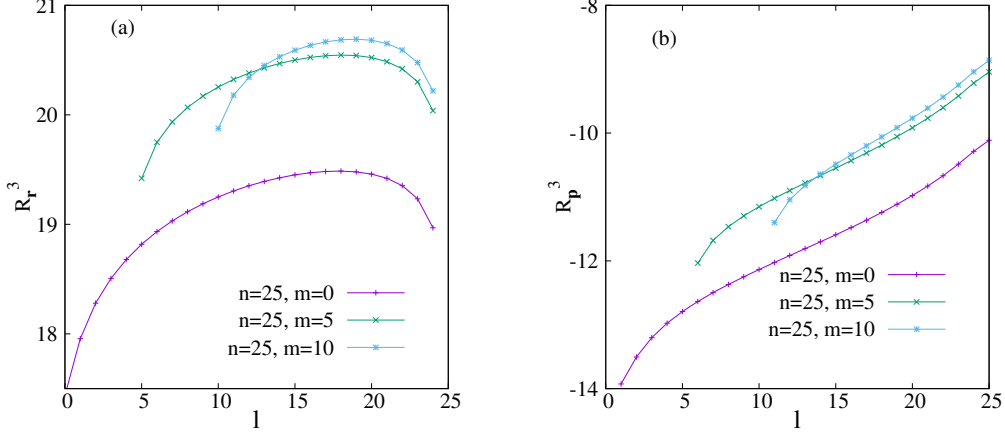


FIG. 4: Changes in R_r^α, R_p^β , in panels (a), (b), with l , for three particular pairs of (n, m) , namely, $(25, 0), (25, 5), (25, 10)$, in a FHA. Both α, β are kept fixed at 3. See text for more details.

only *radial* parts of information measures are presented in tables and figures, whereas for CHA, these correspond to respective *combined* (containing radial and angular) quantities.

A. Free Hydrogen-like atom

We begin by noting that, radial wave function for H-like atoms (in a.u.) in r and p spaces are given in Eqs. (7) and (12) respectively. It is well known [24, 25] that for a single particle in central potential, I_r, I_p are amenable to simple closed-form expressions; former in terms of kinetic energy and radial expectation value $\langle r^{-2} \rangle$, while latter in terms of root-mean square radius and momentum expectation value $\langle p^{-2} \rangle$. For H-like atom, they may be further simplified in terms of n, l, m state indices and Z ,

$$I_r = \frac{4Z^2}{n^2} \left[1 - \frac{|m|}{n} \right], \quad I_p = \frac{2n^2}{Z^2} [(5n^2 + 1 - 3l(l+1)) - |m|(8n - 6l - 3)]. \quad (22)$$

In case of $m = 0$, which we restrict ourselves here, the rightmost term vanishes, leading to,

$$I_r = \frac{4Z^2}{n^2} = 4\langle p^2 \rangle, \quad I_p = \frac{2n^2}{Z^2} [5n^2 + 1 - 3l(l+1)] = 4\langle r^2 \rangle. \quad (23)$$

Thus, like energy, I_r , solely depends on n , whereas, I_p on l , besides n . Thus, it one infers that, I_r, I_p show opposite behavior with n ; former falls down whereas latter grows up. This happens because, as n increases, kinetic energy lowers, whereas mean square root rises. Additionally, at a fixed n , p -space quantity diminishes with growth of l , implying its reduction as number of nodes goes down. In what follows, we give detailed tables of R, T, S, E and not I . However systematic variations in figures cover all of them including I .

TABLE IV: R_r^α and R_p^β for some selected states in FHA ($\alpha = \frac{3}{5}, \beta = 3$). See text for details.

State	R_r^α	R_p^β	State	R_r^α	R_p^β
1s	2.4448978171250	-1.29370300309	10s	15.050243	-12.32498491
2s	6.0819732	-4.8664081148	10p	15.035316	-11.195758752
2p	5.7179773964224	-2.8297112656580	10d	15.005147	-10.57157435657
3s	8.2848709	-6.809107089	10f	14.958899	-10.10288080007
3p	8.1262512	-5.3065985061863	10g	14.894965	-9.700944996180
3d	7.7379345080228	-3.8973824203957	10h	14.810529	-9.32574529
4s	9.8747416	-8.1489547505	10i	14.700625	-8.95119472938
4p	9.7849766	-6.8261191707376	10k	14.555826	-8.55253099
4d	9.5879299	-5.8530683362380	10l	14.355085	-8.0952748
4f	9.2078601178873	-4.7097820569485	10m	14.031044068431	-7.521354

1. Circular states

In this subsection, some exact analytical results are given for the node-less ($n - l = 1$) or so-called *circular* states in a FHA in r, p space. Note that for such states, the two respective polynomials $L_{2l+1}^{n-l-1}(\frac{2Z}{n}r)$ and $C_{n-l-1}^{l+1}(\frac{(\frac{np}{Z})^2-1}{(\frac{np}{Z})^2+1})$ both reduce to unity. Hence radial components of wave functions in r, p spaces simplify to,

$$\begin{aligned}\psi_{n-l=1}(r) &= \frac{2}{n^2} \left[\frac{1}{(n+l)!} \right]^{\frac{1}{2}} \left[\frac{2Z}{n}r \right]^l e^{-\frac{Z}{n}r} \\ \psi_{n-l=1}(p) &= n^2 \left[\frac{2}{\pi} \frac{1}{(n+l)!} \right]^{\frac{1}{2}} 2^{(2l+2)} l! \frac{n^l}{\{[\frac{np}{Z}]^2 + 1\}^{l+2}} \left(\frac{p}{Z} \right)^l.\end{aligned}\tag{24}$$

At first, the radial entropic moments ω_r^α and ω_p^β are calculated using wave functions in Eq. (24) and definition in Eq. (18), leading to following forms,

$$\begin{aligned}\omega_r^\alpha &= \left(\frac{2Z}{n} \right)^{(3\alpha-3)} \left\{ \frac{\Gamma(2l\alpha+3)}{\alpha^{(2l\alpha+3)} [\Gamma(2l+3)]^\alpha} \right\}, \\ \omega_p^\beta &= \left(\frac{n}{Z} \right)^{(3\beta-3)} \left\{ \frac{\Gamma(2l+2)}{\Gamma(\frac{2l+3}{2}) \Gamma(\frac{2l+5}{2})} \right\}^\beta \left\{ \frac{\Gamma(\frac{2l\beta+3}{2}) \Gamma(\frac{2l\beta+8\beta-3}{2})}{\Gamma(2l\beta+4\beta)} \right\}.\end{aligned}\tag{25}$$

Now, routine mathematical manipulation leads to R_r^α and R_p^β as,

$$\begin{aligned}R_r^\alpha &= 3 \ln \left[\frac{n}{2Z} \right] + \frac{(2l\alpha+3)}{(\alpha-1)} \ln \alpha + \frac{1}{(\alpha-1)} [\alpha \ln \{\Gamma(2l+3)\} - \ln \{\Gamma(2l\alpha+3)\}], \\ R_p^\beta &= 3 \ln \left[\frac{Z}{2^{\frac{1}{3}}n} \right] + \frac{1}{(1-\beta)} \left[\beta \ln \left\{ \frac{\Gamma(2l+4)}{\Gamma(\frac{2l+3}{2}) \Gamma(\frac{2l+5}{2})} \right\} + \ln \left\{ \frac{\Gamma(\frac{2l\beta+3}{2}) \Gamma(\frac{2l\beta+8\beta-3}{2})}{\Gamma(2\beta(l+2))} \right\} \right],\end{aligned}\tag{26}$$

TABLE V: T_r^α and T_p^β for some selected states in FHA ($\alpha = \frac{3}{5}, \beta = 3$). See text for details.

State	T_r^α	T_p^β	State	T_r^α	T_p^β
1s	4.14755992475	-6.1476195330	10s	1026.566912	-2.53697×10^{10}
2s	25.9765245	-8430.486351	10p	1020.508405	-2.65144×10^9
2p	22.11809373949	-142.99143553	10d	1008.283591	-7.57534×10^8
3s	66.2336586	-4.104731×10^5	10f	989.659422	-2.98007×10^8
3p	62.0081804	-20333.5038833	10g	964.605525	-1.33389×10^8
3d	52.72769426026	-1213.4292120388	10h	932.546877	-6.29880×10^7
4s	127.32504795	-5.984972×10^6	10i	893.652698	-2.97745×10^7
4p	122.74685003	-4.246794×10^5	10k	841.846208	-1.34213×10^7
4d	113.56339555	-6.0656449×10^4	10l	776.747706	-5.37571×10^7
4f	96.92810090882	-6163.10389494375	10m	682.0134947207	-1.70583×10^6

whereas the **radial PM Rényi entropy** can be written as, $R^{(\alpha,\beta)} = R_r^\alpha + R_p^\beta$.

Equation (26) provides R_r^α , R_p^β for arbitrary α , β . In order to compute **radial PM Rényi entropy** $R^{(\alpha,\beta)}$, the relation ($\frac{1}{\alpha} + \frac{1}{\beta} = 2$) should be satisfied between them. Figure 1 graphically shows variations of R_r^α , R_p^β in panels (a), (b) with α , β respectively, for lowest five node-less states 1s, 2p, 3d, 4f, 5g. It follows that with progression in α, β , both R_r^α , R_p^β lessen for all of them. Further, R_r^α 's, R_p^β 's appear to behave contrastingly with upward changes in n, l ; former assume progressively higher values, while latter go down. Starting from an initial value, all these fall quite sharply in lower α, β regions and tend to flatten as the latter two widen. Moreover, the extent of fall-off slows down as n, l tend to grow.

Now, Fig. 2 displays the plots of R_r^α, R_p^β and **radial PM Rényi entropy** $R^{(\alpha,\beta)}$, with n at three chosen sets of α ($\frac{3}{5}, 1, 3$), β ($\frac{3}{5}, 1, 3$) and (α, β) , namely $(\frac{3}{5}, 3), (1, 1), (3, \frac{3}{5})$ in three panels (a)-(c). Recall that, the above R 's corresponding to set $\alpha = \beta = 1$ represent S_r, S_p , **radial PM Shannon entropy** S respectively. While range of n remains fixed in all three plots, same for y axis differs in all cases. For all α , R_r^α 's rise with n —more sharply at smaller n 's, See text for details. and rate of progress taking a dive with n . At a given n , R_r^α tends to diminish continuously as order of moment enhances. On the other hand, R_p^β in (b) shows a complimentary behavior to (a), steadily falling as n grows. A combined effect of these two produces the plot in panel (c), quite similar in qualitative nature as in (a), with visible differences in the values in y axis. Since α, β obey the relation $\frac{1}{\alpha} + \frac{1}{\beta} = 2$, when $\alpha > 1$, $\beta < 1$ and vice versa. Evidently, in both situations, corresponding changes in $R_r^\alpha, R_p^\beta, R^{(\alpha,\beta)}$ maintain similar trend. The above reasoning may be interpreted in terms of

TABLE VI: S_r, S_p for some selected states in FHA. See text for details.

State	S_r^\dagger	S_p^\dagger	State	S_r^\S	S_p^\S
1s [†]	1.6137056388801	-0.1091619058	10s	14.83421801	-8.5831
2s	5.579905117	-3.288603	10p	14.81546079	-8.40306
2p	5.1658184934843	-2.056657825	10d	14.779519706	-8.22058
3s	7.895456983	-4.71928	10f	14.726933588	-8.03408
3p	7.706768439	-3.988042	10g	14.657200818	-7.84526
3d	7.3045091959407	-3.273842250	10h	14.568453746	-7.65744
4s	9.543883432	-5.67677	10i	14.456574316	-7.47587
4p	9.434788623	-5.162422	10k	14.312835432	-7.30982
4d	9.220979188	-4.635591	10l	14.116240399	-7.1796
4f	8.8401955766914	-4.169046134	10m	13.794498337697	-7.1533

[†]Literature results [37] for $S_r = S_r + S_{(\theta, \phi)}$ and $S_p = S_p + S_{(\theta, \phi)}$ are 4.1447 and 2.4219 respectively. Present values are 4.14472988585 and 2.42186234117.

[‡]Literature results [35] of S_r, S_p for 1s-4f states are: (1.6137056388, -0.1091619058), (5.5799051176, -3.2886034474), (5.1658184934, -2.0566578254), (7.8954569837, -4.7192844860), (7.7067684395, -3.9880420674), (7.3045091959, -3.2738422502), (9.5438834322, -5.6767751478), (9.4347886234, -5.1624221872), (9.2209791882, -4.6355912037), (8.8401955766, -4.1690461340) respectively.

[§]Literature results [35] of S_r, S_p for 10s-10m states are: (14.834218018, -8.583082598), (14.815460797, -8.403065247), (14.779519706, -8.220588961), (14.726933588, -8.034081080), (14.657200818, -7.845266303), (14.568453746, -7.657443887), (14.456574316, -7.475870737), (14.312835432, -7.309826844), (14.116240399, -7.179685623), (13.794498337, -7.153386777) respectively.

radial probability distribution getting more diffused with n . It is appropriate to mention here that, the bounds provided in Eqs. (14), (15) and (19) are applicable to total PM Fisher information, total PM Shannon entropy and total PM Rényi entropy. Thus, in case of FHA, the *radial* PM Rényi, PM Shannon entropy and PM Onicescu energies, reported here, are not subject to such bounds.

Next we proceed for T_r^α and T_p^β , which are obtained from Eq. (20) as,

$$\begin{aligned}
 T_r^\alpha &= \frac{1}{\alpha - 1} \left[1 - \left(\frac{2Z}{n} \right)^{(3\alpha-3)} \left\{ \frac{\Gamma(2l\alpha + 3)}{\alpha^{(2l\alpha+3)} [\Gamma(2l + 3)]^\alpha} \right\} \right], \\
 T_p^\beta &= \frac{1}{\beta - 1} \left[1 - 2^{(\beta-1)} \left(\frac{n}{Z} \right)^{(3\beta-3)} \left\{ \frac{\Gamma(2(l+2))}{\Gamma\left(\frac{2l+3}{2}\right) \Gamma\left(\frac{2l+5}{2}\right)} \right\}^\beta \left\{ \frac{\Gamma\left(\frac{2l\beta+3}{2}\right) \Gamma\left(\frac{2l\beta+8\beta-3}{2}\right)}{\Gamma(2\beta l + 4\beta)} \right\} \right].
 \end{aligned} \tag{27}$$

Evidently, T_r^α, T_p^β show analogous behavior as R_r^α, R_p^β in Eq. (26), namely, T_r^α grows up, whereas T_p^β reduces with successive upward changes in n . A characteristic feature of R, T is that, when $(\alpha, \beta) \rightarrow 1$ we have $(R_r^\alpha, T_r^\alpha) \rightarrow S_r$ and $(R_p^\beta, T_p^\beta) \rightarrow S_p$. Therefore we

TABLE VII: E_r and E_p for some selected states in FHA. See text for details.

State	E_r	E_p	State	E_r	E_p
1s	0.5	2.626056561016	10s	0.000000943317	93503.5290
2s	0.009765625	96.1295856275048	10p	0.000000841581	39072.5385
2p	0.001398822737580	13.793428401297597	10d	0.000000801822	23397.786166
3s	0.000964506172839	599.4570931556239	10f	0.000000785289	15697.1858628
3p	0.000884130658436	160.07008401467374	10g	0.000000784339	11036.824894
3d	0.001012731481481	41.63970776113258	10h	0.000000797955	7885.727210
4s	0.000185489654541	2072.833978828845	10i	0.000000829206	5609.7326559
4p	0.000166416168212	676.412752272371	10k	0.000000887467	3899.8392585
4d	0.000170230865478	277.6680799158443	10l	0.000000999887	2595.614180
4f	0.000204563140869	95.71851114591887	10m	0.000001285853	1659.760152

employ Eqs. (26), (27) separately (both lead to same result obviously) in this limit to secure following expressions for S_r, S_p in node-less states, *viz.*,

$$S_r = 3 \ln \left[\frac{n}{2Z} \right] + (2l + 3) + \ln[\Gamma(2l + 3)] - 2l \left[\sum_{k=1}^{2l+2} \left(\frac{1}{k} \right) - C \right],$$

$$S_p = \ln \left[\frac{Z^3}{2n^3} \frac{\Gamma\left(\frac{2l+3}{2}\right) \Gamma\left(\frac{2l+5}{2}\right)}{\Gamma(2l+4)} \right] - l \frac{\Gamma'\left(\frac{2l+3}{2}\right)}{\Gamma\left(\frac{2l+3}{2}\right)} - (l+4) \frac{\Gamma'\left(\frac{2l+5}{2}\right)}{\Gamma\left(\frac{2l+5}{2}\right)} + (2l+4) \frac{\Gamma'(2l+2)}{\Gamma(2l+2)}.$$
(28)

Here $\frac{\Gamma'(t)}{\Gamma(t)}$ refers to the Poly-Gamma function with order 0, and Euler Constant C equals to 0.57721 56649 01532 86060 651209... The **radial PM Shannon entropy** S is then gathered as sum of individual components S_r and S_p .

Additionally, we have derived S_r, S_p for such states using an alternate method applying the definition in Eq. (16). It turns out that the analytical expression of S_r obtained from this route is completely identical to that in Eq. (28). However for S_p , one obtains the following expression from Eq. (16),

$$S_p = \ln \left[\frac{Z^3 \Gamma\left(\frac{2l+3}{2}\right) \Gamma\left(\frac{2l+5}{2}\right)}{2n^3 \Gamma(2l+4)} \right] + \left[\frac{\sqrt{\pi} l \Gamma(2l+3)}{2^{(2l+2)} \Gamma(l+2) \Gamma\left(\frac{2l+5}{2}\right)} \right] + (4l+8) \left[\frac{\Gamma(2l+4)}{\Gamma\left(\frac{2l+5}{2}\right) \Gamma\left(\frac{2l+3}{2}\right)} \right] I_p^l.$$
(29)

The integration in last line is defined as given below,

$$I_p^l = \int_0^\infty \frac{p^{(2l+2)}}{(1+p^2)^{(2l+4)}} \ln(1+p^2) dp,$$
(30)

which can be computed for a specific l numerically quite easily.

Table S1, however, demonstrates that the two expressions of S_p , in Eqs. (28) and (29), although apparently different, actually produce virtually identical numerical results. Here

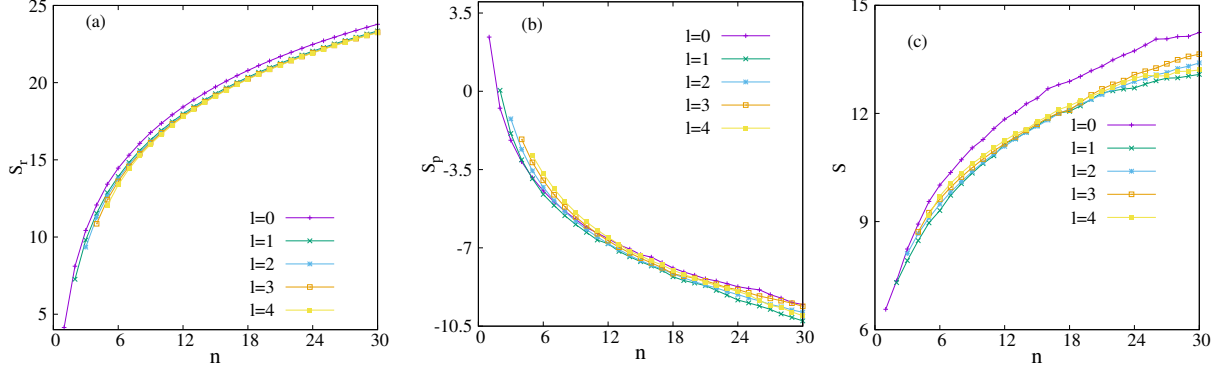


FIG. 5: Changes in S_r, S_p , **radial PM Shannon entropy S** with n at five lowest l (0-4) in FHA. For more details, see text.

we offer lowest eleven node-less states for the purpose of illustration, but this has been found to be generally valid for other states as well. One can surmise that S_p falls down steadily as n rises. Further, the graphs $\alpha = 1$ and $\beta = 1$ in panels (a), (b) of Fig. 2 endorse that, for circular states, S_r rises and S_p diminishes with n advancing forward.

From the foregoing analysis, it is realized that, R_r^α, T_r^α and S_r gain with n . Conversely, $R_p^\beta, T_p^\beta, S_p$ assume reverse trend with n . Because, in circular states, the r -space density gets more diffused as n, l progress, without changing number of nodes. Finally, we move on to E in such states in FHA, keeping in mind that, $\alpha = \beta = 2$ in **Eq. (25)** leads to radial Onicescu energy in position (E_r) and momentum (E_p) spaces respectively. After some straightforward algebraic manipulation, one gets,

$$\begin{aligned}
 E_r &= \left(\frac{2Z}{n}\right)^3 \left[\frac{\Gamma(4l+3)}{2^{(4l+3)} \Gamma(2l+3)^2} \right], \\
 E_p &= 2 \left(\frac{n}{Z}\right)^3 \left[\frac{\Gamma(2(l+2))}{\Gamma\left(\frac{2l+3}{2}\right) \Gamma\left(\frac{2l+5}{2}\right)} \right]^2 \left[\frac{\Gamma\left(\frac{4l+3}{2}\right) \Gamma\left(\frac{4l+13}{2}\right)}{\Gamma(4l+8)} \right].
 \end{aligned} \tag{31}$$

One discerns from **Eq. (31)** that, E_r declines whereas E_p grows as n rises. This is in accordance with our previous conclusion that, delocalization escalates, as n becomes larger.

2. States with arbitrary n, l

This subsection is now devoted to a discussion of S, R, T, E for an *arbitrary* state (not necessarily *circular*) in a FHA. Several attempts were made to derive analytical results for S, R, T, E in such states. The main problem remains rooted in integrating the occurring

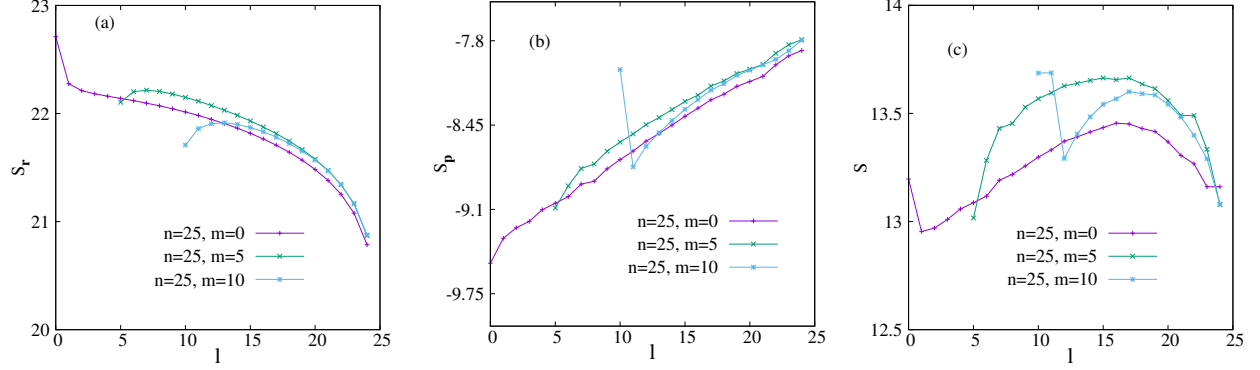


FIG. 6: Variation of S_r , S_p and **radial PM Shannon entropy S** respectively, in panels (a), (b), (c), with l , for three specific pairs of (n, m) , namely, $(25, 0)$, $(25, 5)$, $(25, 10)$, in a FHA. More details are available in the text.

polynomials with certain power (α or β) for R, T or in logarithmic form for S . These functions are exactly integrable when α, β are integers (as they assume finite form). In same token, E ($\alpha = \beta = 2$) for FHA can be written analytically for integer α, β for all states—though for larger n, l , number of contributing terms in polynomial appearing in wave function populates considerably, making it rather cumbersome. However, for fractional α, β , these (R, T) lead to infinite series; hence become quite intractable. Some recent works [29, 31] have reported a few analytical expressions of R with particular approximations in terms of Airy and Bessel functions, for $l = 0$ states of a D-dimensional H-like atom in r space.

Before going to a detailed analysis, at first in **Table III** we present the angular parts of concerned information quantities, *viz.*, $S_{(\theta, \phi)}$, $R_{(\theta, \phi)}^\alpha$, $R_{(\theta, \phi)}^\beta$, $T_{(\theta, \phi)}^\alpha$, $T_{(\theta, \phi)}^\beta$, $E_{(\theta, \phi)}$ in columns 2-7 in a H atom. These are offered for 10 lowest states, keeping m fixed at 0, with specific set of α, β corresponding to $\frac{3}{5}, 3$ respectively. It may be noted that all future calculations employ same α, β . **So far such results are only known for $S_{\theta, \phi}$ [35], where the wave functions were expanded in cut-off STOs and Löwdin's canonical orthogonalization method was used. Our computed $S_{\theta, \phi}$ values are in complete consistence with these results (given below the Table III). But, no reported results are available for $R_{(\theta, \phi)}^\alpha, R_{(\theta, \phi)}^\beta, T_{(\theta, \phi)}^\alpha, T_{(\theta, \phi)}^\beta, E_{(\theta, \phi)}$, to the best of our knowledge.** Their deviations with respect to numerical parameters were carefully checked and are reported here up to the extent to which convergence was attained. These would be applicable to both FHA and CHA, as we are interested only in radial confinement. It is seen that, $S_{(\theta, \phi)}$ as well as p -space components of R, T , i.e., $R_{(\theta, \phi)}^\beta, T_{(\theta, \phi)}^\beta$ gradually fall off as l grows, while an opposite behavior is recorded for $E_{(\theta, \phi)}$; in both occasions the extent is

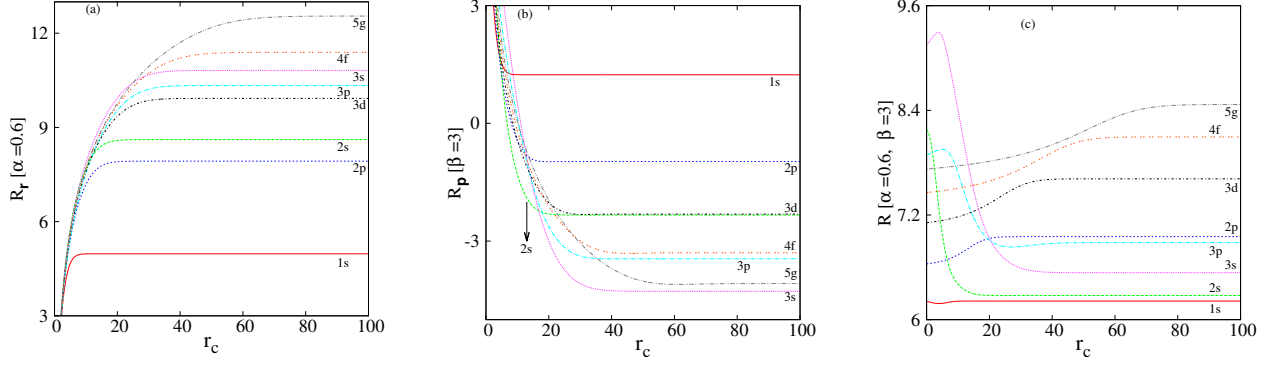


FIG. 7: Plot of R_r^α , R_p^β , **total PM Rényi entropy $R^{(\alpha,\beta)}$** against r_c for some low-lying states of CHA, having $\alpha = \frac{3}{5}, \beta = 3$, in panels (a), (b), (c) respectively. **$R^{(\alpha,\beta)}$'s for all these states obey the lower bound condition given in Eq. (19).** More details can be found in text.

lowered as we go down the table. It is interesting to observe that, both $R_{(\theta,\phi)}^\alpha$, $T_{(\theta,\phi)}^\alpha$ initially decline, then attain minima at $l = 7$ and again tend to ascend thereafter.

Let us now focus on the nature of radial parts of such information quantities. Figure 3 presents rise, fall of R_r^α , R_p^β respectively with changes of n in panels (a), (b) for FHA in case of lowest five l states. This time, we have chosen $\alpha = \beta = 3$. Both quantities assume larger value with l for a given n . This may occur due to spreading of state function with n, l . Also, separation amongst l widens as n goes up. Further, Fig. 4 depicts changes in R_r^α , R_p^β with l keeping n fixed (25) at three different m namely, 0, 5, 10, for same α, β of previous figure. Note that, unlike other figures of FHA, here the graphs include angular contributions. In each of these three m , one finds a hump in (a) segment, all passing through a maximum. Whereas right side reveals that R_p^β climbs up with l . It may be noted that, for a fixed n , number of radial nodes lowers as l increments. On the other hand, if n is sufficiently large (which is the case here), radial orbitals get comparably (and considerably as well) extended amongst all available l . Now, from discussion of **Table III**, we know that, with l , angular contribution initially grows up, then attains a maximum and in the end falls down. Thus it is not quite straightforward to explain such graphs. Rather, these calculations may be used to grasp the distribution pattern of total probability in high- n, l states.

Now we turn to the main results of FHA. **Table IV** provides our numerically estimated values for R_r^α, R_p^β in left portion, for $1s-4f$ states, while right side correspond to those for all ten l states belonging to $n = 10$. Left, right side of **Table V** display similar entries for T_r^α, T_p^β , for above same states, while results for S_r, S_p and E_r, E_p are tabulated in

Tables VI and VII. Except for the case of S_r, S_p in Table VI, all these are offered here for first time and we hope they would be useful for future referencing and stimulate further research in this direction. Literature result for S_r, S_p is based on a variational calculation [35, 37], which shows reasonable agreement with our present finding. Note that reference data of [37] correspond to $S_{\mathbf{r/p}}$ rather than $S_{r/p}$; therefore need to be adjusted for their appropriate angular contributions $S_{(\theta, \phi)}$. At this point, it may be recalled that, a lowering and raising in R, T, S reflects global extension and concentration of density distribution in corresponding spaces. It is noticed from Tables IV-VI that, for all n considered, R, T, S diminish and progress in r, p spaces as l ascends. On the other hand, Table VII suggests that, for a specific l , E_r and E_p show contrasting behavior (fall, rise respectively) with n , which could be attributed to a gain in number of radial nodes, leading to a delocalization of electron. Interestingly, as l changes for a given n , E_r at first drops down, attains a minimum before surging further. Conversely, for same reason, E_p descends with growth of l . This time, number of radial nodes dips, but with l going up, there is a spread in probability distribution. Due of these two contrasting factors, one encounters inflection points in E_r .

Figure 5 now registers nature of changes in S_r (a), S_p (b), radial PM Shannon entropy S (c) with n at first five l (0 – 4). Evidently, S_r, S tend to grow with n , whereas S_p shows reverse effect. This is in keeping with that, as n, l are raised, radial orbitals get extended in space. It is worth pointing out that unlike R, S_r and S slump with l . But, S_p does not permit any straightforward motif.

Next Fig. 6 depicts modulation of S_r, S_p , radial PM Shannon entropy S in left, middle, right segments (a)-(c), with changes in l , keeping n fixed (25) at three distinct m , namely, 0, 5, 10. Unlike $R_{\mathbf{p}}^3$, of Fig. 4, S_r for $m = 0$ changes inversely with l . But, for the other two m , like $R_{\mathbf{r}}^3$ of Fig. 4, S_r 's advance with l , attain some plateau and then decline. On the other hand, S_p 's for first two m , follow the same trend as $R_{\mathbf{p}}^3$ did. In both cases, S_p 's steadily upturn with l . Only, for $m = 10$, it deviates from $R_{\mathbf{p}}^3$ and shows a downward trend reaching a minimum, and then climbing up again. For S , one encounters a plateau for $m = 0, 5$, whereas, for $m = 10$, first there appears a maximum followed by a minimum and lastly a plateau. Like the R plots of Figs. 3, 4, in this case also, while n variations are rather direct and straightforward, same for l are relatively intricate. However, like Fig. 4, this result may also be useful to understand transmission of total probability distribution of atomic orbitals.

TABLE VIII: $R_{\mathbf{r}}^{\alpha}$, $R_{\mathbf{p}}^{\beta}$ and **total PM Rényi entropy** $R^{(\alpha,\beta)} = (R_{\mathbf{r}}^{\alpha} + R_{\mathbf{p}}^{\beta})$ for lowest two s states in a CHA, at various r_c , for $\alpha = \frac{3}{5}, \beta = 3$ respectively. See text for more details.

1s				2s			
r_c	$R_{\mathbf{r}}^{\alpha}$	$R_{\mathbf{p}}^{\beta}$	$R^{(\alpha,\beta)}$	r_c	$R_{\mathbf{r}}^{\alpha}$	$R_{\mathbf{p}}^{\beta}$	$R^{(\alpha,\beta)}$
0.1	-6.0449530234201	12.2544945	6.2095414	0.1	-6.0652785667052	14.2461812	8.18090263
0.2	-3.9740686542021	10.1826733	6.20860464	0.2	-3.9857010841026	12.1605425	8.17484143
0.3	-2.7665379461615	8.97420833	6.20767038	0.3	-2.7690858567973	10.9370670	8.16798114
0.5	-1.2527639276520	7.4585759	6.20581197	0.5	-1.2359050275123	9.3875148	8.15160977
0.6	-0.7156642633591	6.9205535	6.2048892	0.6	-0.6884504327452	8.83042433	8.1419738
0.8	0.1265545289041	6.0765062	6.2030607	0.8	0.1758653404988	7.9436427	8.1195080
1.0	0.7735958787514	5.4276644	6.20126027	1.0	0.8469685980263	7.2454746	8.0924431
1.5	1.9263580259098	4.27057585	6.19693387	3.0	4.1824208766826	3.3944866	7.5769074
2.5	3.2916372871390	2.89792262	6.18955990	5.0	5.7661541562104	1.2155313	6.9816854
3.0	3.7310884276653	2.45579844	6.1868868	7.5	6.9655961664353	-0.3916768	6.5739193
4.0	4.3257559261586	1.85876674	6.1845226	10.0	7.7053107207956	-1.2984101	6.4069006
5.0	4.6620663954973	1.5246585	6.1867248	12.0	8.0874246952222	-1.7443702	6.3430544
7.5	4.9391522549392	1.2635057	6.20265795	15.0	8.4139254912730	-2.1168056	6.2971198
10.0	4.9726811434694	1.23872097	6.21140211	20.0	8.5857873091459	-2.3081634	6.27762390
20.0	4.9759220330329	1.23732124	6.21324327	30.0	8.6127521696429	-2.33524516	6.27750700
40.0	4.9759220625078	1.23732124	6.21324330	40.0	8.6129969633475	-2.33538378	6.27761318

B. The confined Hydrogen atom

In this subsection now, all information measures of previous subsection are presented, in case of a CHA, in order to help uncover the impact of impenetrable spherical cage on these. The radial boundary now changes from infinity to a finite region without affecting angular boundary conditions. Thus, angular information contributions, as produced in [Table III](#), remain invariant to a change in potential from FHA to CHA. It is expected that, a progressively larger r_c should lead to a delocalization in the system in such a fashion that, when $r_c \rightarrow \infty$, it should evolve to FHA. Whereas, when $r_c \rightarrow 0$, influence of confinement is maximum. Thus, it will be convenient to pursue our calculation by choosing some specific r_c values starting from 0.1 to 100. This parametric increase in r_c reveals manifestation of the system from maximum confinement to a free system.

To begin with, [Table VIII](#) displays calculated $R_{\mathbf{r}}^{\alpha}$, $R_{\mathbf{p}}^{\beta}$, **total PM Rényi entropy** $R^{(\alpha,\beta)}$ for 1s, 2s states of CHA, at a selected set of r_c ; which differ for the two. In this and all following tables of CHA, information quantities are furnished for these two states. In order to save space and volume of the length of this communication, higher states (especially having non-

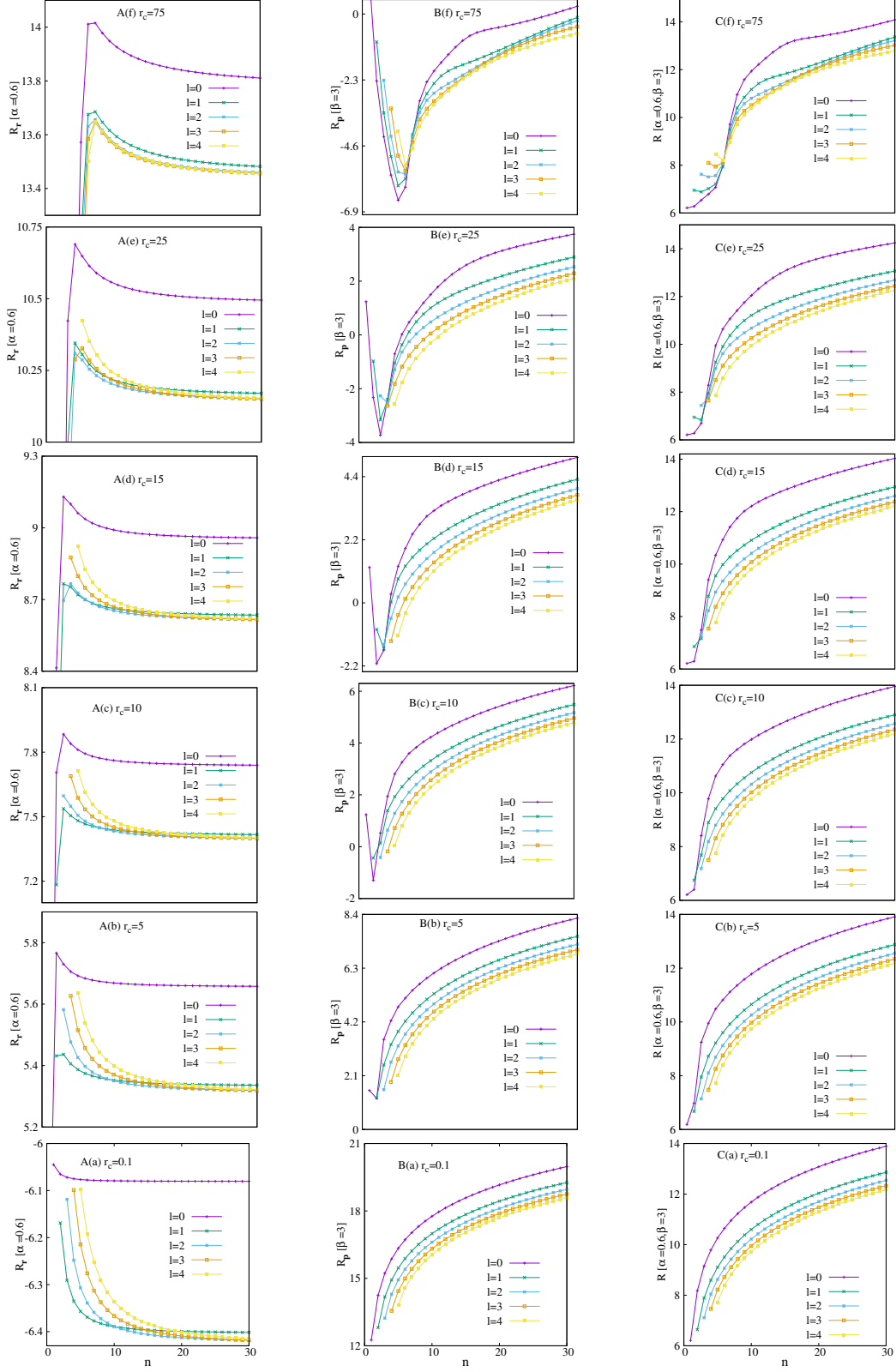


FIG. 8: Plot of R_r^α (A), R_p^β (B) and total PM Rényi entropy $R^{(\alpha,\beta)}$ (C) versus n for s, p, d, f, g orbitals at six particular r_c values of CHA, namely, 0.1, 5, 10, 15, 25, 75 in panels (a)-(f). $R^{(\alpha,\beta)}$'s for all these states obey the lower bound given in Eq. (19). For more details, consult text.

zero l) are omitted and may be presented elsewhere in future. This does not affect the main theme of this work. However, to facilitate a clear understanding and presentation, these are well included in plots where required. In both occasions, $R_{\mathbf{r}}^{\alpha}$'s, starting from certain negative values at very small r_c , continuously progress, finally converging to the respective FHA behavior after some larger finite r_c . In contrast, $R_{\mathbf{p}}^{\beta}$'s in both states generally tend to diminish with r_c , again merging to FHA in the end. In $2s$, eventually it goes to the $(-)$ ve in large r_c . Consequently, the **total PM Rényi entropy** for $1s$, depletes with r_c and goes through a minimum before attaining FHA. For $2s$, however, it decays with r_c to reach the borderline value. For two states under consideration, these convergences occur at roughly $r_c \approx 20, 30$ respectively. At very low r_c , $R_{\mathbf{r}}^{\alpha}(1s) > R_{\mathbf{r}}^{\alpha}(2s)$ but they cross each other at around $r_c \approx 0.4$. A similar exercise leads to $R_{\mathbf{p}}^{\beta}(2s) > R_{\mathbf{p}}^{\beta}(1s)$ at smaller r_c , with crossing occurring at nearly $r_c \approx 4 - 5$. There is no such crossover in $R^{(\alpha,\beta)}$ in any of these states. No literature results could be found for these quantities to make direct comparison. Above observations are vividly depicted in Fig. 7, where in three segments, (a)-(c), changes in $R_{\mathbf{r}}^{\alpha}$, $R_{\mathbf{p}}^{\beta}$, **total PM Rényi entropy** $R^{(\alpha,\beta)}$ of representative eight (covering 3 zero- and 5 non-zero- l) states, *viz.*, $1s, 2s, 2p, 3s, 3p, 3d, 4f, 5g$ of CHA, with respect to r_c are recorded. Panel (a) reveals that, for all of them, $R_{\mathbf{r}}^{\alpha}$'s quite smoothly advance initially with r_c , and finally coalesce to FHA. Likewise, from panel (b), clearly, $R_{\mathbf{p}}^{\beta}$ shows a reverse behavior with r_c , before reaching FHA-limit. Panel (c) portrays that for $1s$, $R^{(\alpha,\beta)}$ in the beginning, shows a drop with r_c , then attains a minimum, and decisively converges to limiting value of 6.213243 at nearly $r_c \approx 10$, whereas for $2s$, it continuously falls off as r_c extends, and thereafter reaching the FHA value of 6.2776 at around $r_c \approx 20$. For $3s, 3p$ states $R^{(\alpha,\beta)}$'s first rise with r_c , then attain some maxima and decay until reaching FHA. For remaining node-less states, $R^{(\alpha,\beta)}$'s register growth with r_c , before permanently marching towards FHA. This characteristic r_c generally shifts towards right, as n moves upwards. It is important to note that, there appears multiple crossovers amongst various states in all these entropies, which occurs due to confinement. A more detailed, systematic study would be necessary to explain the pattern of this occurrence, which may be undertaken in future.

To gain further insight, Fig. 8 portrays $R_{\mathbf{r}}^{\alpha}, R_{\mathbf{p}}^{\beta}$, **total PM Rényi entropy** $R^{(\alpha,\beta)}$ in left (A), middle (B), right (C) panels, for lowest five l (0–4) as function of n , (maximum of 30). Six different r_c 's are chosen, i.e., 0.1, 5, 10, 15, 25, 75, in segments (a) through (f) from bottom to top. At $r_c = 0.1$, for all l , $R_{\mathbf{r}}^{\alpha}$'s consistently go down with n , while $R_{\mathbf{p}}^{\beta}, R^{(\alpha,\beta)}$ show opposite

TABLE IX: $T_{\mathbf{r}}^{\alpha}, T_{\mathbf{p}}^{\beta}$ and **total PM Tsallis entropy** $T^{(\alpha,\beta)} (= T_{\mathbf{r}}^{\alpha} T_{\mathbf{p}}^{\beta})$ for 1s and 2s states, at several particular r_c in a CHA, for $\alpha = \frac{3}{5}, \beta = 3$ respectively. Consult text for more details.

1s				2s			
r_c	$T_{\mathbf{r}}^{\alpha}$	$T_{\mathbf{p}}^{\beta}$	$T^{(\alpha,\beta)}$	r_c	$T_{\mathbf{r}}^{\alpha}$	$T_{\mathbf{p}}^{\beta}$	$T^{(\alpha,\beta)}$
0.1	-2.2772467171115	0.499999999988	-1.138623358529	0.1	-2.27905040787	0.499999999997	-1.139525203938
0.2	-1.9899960082576	0.499999999284	-0.994998002705	0.2	-1.99236352845	0.499999999863	-0.996181764197
0.5	-0.9853488252731	0.499999833837	-0.492674248908	0.5	-0.97510014910	0.4999999964918	-0.487550071130
0.8	0.1298124908784	0.499997363767	0.064905903223	0.8	0.18219873857	0.4999999370189	0.091099357813
1.0	0.9066489220414	0.499990349260	0.453315711188	1.0	1.00811263141	0.4999997455334	0.504056059175
1.5	2.9023494698347	0.499902367380	1.450891370935	3.0	10.81989915020	0.4994369378358	5.403857299273
2.5	6.8273006148635	0.498479920188	3.403272265597	5.0	22.59710251821	0.4560283384851	10.30491911595
5.0	13.6370406555684	0.476304362681	6.495381958317	7.5	38.04973331016	-0.59440039327	-22.61677644352
10.0	15.7718785921688	0.458021139475	7.223853804451	15.0	69.87499964359	-33.9829209887	-2374.556591979
20.0	15.7955808066365	0.457903457550	7.232851065381	30.0	75.86611269904	-52.8750365859	-4011.423484596
40.0	15.7955810228201	0.457903457462	7.232851162970	40.0	75.87378643375	-52.8898370490	-4012.952200777

trend. Furthermore, they follow similar pattern with l , for a given n . This indicates that, at small r_c , effect of confinement is more pronounced for high- n, l states implying that, quantum nature gets amplified in this situation. Because, information content reduces, whereas PM information (uncertainty) escalates. First two columns (A, B), interestingly show appearance of a maximum, minimum in $R_{\mathbf{r}}^{\alpha}, R_{\mathbf{p}}^{\beta}$ plots with regular advancement of r_c , as one moves up from bottom (a) to top (f) panel. Positions of these maxima, minima move to right as r_c intensifies. Apparently, there exists an interplay between two competing aspects: (i) radial confinement (localization) and (ii) accumulation in the nodes with n (delocalization). With a build-up in r_c , delocalization predominates for lower n , whereas extent of localization is more prominent for larger n . Hence with steady relaxation of confinement, states having greater n get delocalized. In the limit of $r_c \rightarrow \infty$, where second effect prevails, system behaves as FHA, with the plots reducing to Figs. 3(a), 3(b) respectively. Third column portrays that, in all six r_c 's, $R^{(\alpha,\beta)}$'s strengthen with n . In all cases, $l = 0$ plots remain rather isolated from all higher l , which within themselves form a family.

Next, **Table IX** reports numerical values of $T_{\mathbf{r}}^{\alpha}, T_{\mathbf{p}}^{\beta}$, **total PM Tsallis entropy** $T^{(\alpha,\beta)}$ for first two s states of CHA at several distinct r_c . These are selected so as to cover small, moderate and large cage radius. Once again, no reference work exists for these, which could be compared. Here, starting from a (-)ve value, $T_{\mathbf{r}}^{\alpha}$'s continually progress with r_c for both states, and in the end, merge with FHA. The same for $T_{\mathbf{p}}^{\beta}$'s, from an initial value of 0.5,

TABLE X: S_r, S_p , total PM Shannon entropy S for $1s, 2s$ states in CHA at some chosen r_c . S 's for all these states obey the lower bound given in Eq. (15). See text for details.

1s				2s			
r_c	S_r	S_p	$S = S_r + S_p$	r_c	S_r	S_p	$S = S_r + S_p$
0.1 [§] , ¶	-6.2445033842373	12.8535	6.6089	0.1	-6.4474579193881	14.638	8.1905
0.2 ¶	-4.1778564051631	10.7787	6.6008	0.2*	-4.3692335356773	12.5593	8.1900
0.3	-2.9747379859399	9.5675	6.5927	0.3	-3.1539053277870	11.343	8.189
0.5 [§] , †, ¶	-1.4703406847180	8.0472	6.5768	0.5	-1.6230786943140	9.8112	8.1881
0.6 ¶	-0.9382193800580	7.5073	6.5890	0.6*	-1.0766799706228	9.2647	8.1880
0.8	-0.1065724371260	6.6609	6.5543	0.8	-0.2142040627489	8.4027	8.1884
1.0 [§] , †, ‡, ¶	0.5290303076727	6.0114	6.5404	1.0 *	0.4554622941859	7.7347	8.1901
1.5	1.6490560732453	4.8627	6.5117	3.0*	3.8083926260850	4.454	8.262
2.5	2.9291995226882	3.562952	6.492151	5.0*	5.4641608279724	2.8173	8.2814
3.0 [†] , ‡, ¶	3.3163654395398	3.1801450	6.496510	7.5	6.7230262418630	1.3022	8.025
4.0	3.7942454904008	2.7241362	6.5183816	10.0*	7.4461562639086	0.2765	7.7226
5.0 [†] , ¶	4.0174441862565	2.5243610	6.5418051	12.0	7.7816678917348	-0.23875	7.54291
7.5	4.1393245365993	2.42550824	6.5648327	15.0	8.0218565650054	-0.6283	7.3935
10.0 ¶	4.1446014364987	2.42193665	6.56653808	20.0*	8.1057256203059	-0.75320	7.35252
20.0	4.1447298842431	2.42186233	6.56659221	30.0*	8.1109253338427	-0.75758	7.35334
40.0 ¶	4.1447298842432	2.42186233	6.56659221	40.0	8.1109293629546	-0.75758	7.35334

[§]Literature results [37] of (S_r, S_p, S) at $r_c = 0.1, 0.5, 1$ in $1s$ state are: $(-6.2445, 12.8536, 6.6091)$, $(-1.4702, 8.0473, 6.5771)$ and $(0.5290, 6.0115, 6.5405)$ respectively.

[†]Literature results [34] of (S_r, S_p, S) at $r_c = 0.5, 1, 3, 5$ in $1s$ state are: $(-1.47, 7.967, 6.497)$, $(0.529, 5.991, 6.52)$, $(3.316, 3.183, 6.499)$ and $(4.011, 2.533, 6.544)$ respectively.

[‡]Literature results [36] of (S_r, S_p, S) at $r_c = 1, 3$ in $1s$ state are: $(0.52903, 6.011673, 6.54703)$ and $(3.316365, 3.180236, 6.496602)$ respectively.

¶Literature results [35] of (S_r, S_p, S) at $r_c = 0.1, 0.2, 0.5, 0.6, 1, 3, 5, 10, 40$ in $1s$ state are:

$(-6.24450338251, 12.85356277, 6.60905939)$, $(-4.1778564034, 10.77871310, 6.60085670)$, $(-1.47034068299, 8.04723315, 6.57689247)$, $(-0.9382193783, 7.50740813, 6.56918875)$, $(0.52903030941, 6.01144522, 6.54047553)$, $(3.31636544150, 3.18014501, 6.49651045)$, $(4.01744418917, 2.52436106, 6.54180525)$, $(4.14460144459, 2.42193666, 6.56653810)$, $(4.14472988585, 2.42186234, 6.56659222)$ respectively.

*Literature results [35] of (S_r, S_p, S) at $r_c = 0.2, 0.6, 1, 3, 5, 10, 20, 30$ in $2s$ state are: $(-4.3692335342, 12.55940257, 8.19016903)$, $(-1.076679969, 9.26455393, 8.18787396)$, $(0.4554622961, 7.73472053, 8.19018283)$, $(3.8083926278, 4.45432335, 8.26271598)$, $(5.4641608298, 2.8174878158, 8.28164864)$, $(7.4461562656, 0.27655185, 7.72270812)$, $(8.1057256268, -0.75319646, 7.35252916)$, $(8.1109253319, -0.75758021, 7.35334511)$ respectively.

steadily fall off with r_c before reaching the same fate of attaining FHA limit. While the change is rather mild for $1s$ for entire range, for $2s$, it is quite dramatic, especially around $r_c \approx 7.5$, from where it becomes $(-)$ ve, and approach very large magnitude at the end. Like R_r^α , at very low r_c , $T_r^\alpha(1s) > T_r^\alpha(2s)$ but at nearly $r_c \approx 0.4$, they cross each other. Initially, in lower r_c , $T_p^\beta(2s) > T_p^\beta(1s)$; the ordering reverses in the r_c range of 4-5. There

is a fundamental difference in the nature of $T^{(\alpha,\beta)}$ of these states however; from a $(-)$ ve value, ground state gradually progresses steadily, while in $2s$, it passes through a positive maximum, joining two terminal negatives. For further appreciation, panels (a)-(c) of [Fig. S1](#) reveal corresponding changes of Tsallis entropies with respect to r_c , in same eight states as in [Fig. 7](#). In all occasions, T_r^α 's tend to enlarge in great extent with r_c and at last coalesce to FHA. Panel (b), on the other hand gives an opposite effect for T_p^β . Actually, for all states, they dip as r_c grows up and eventually converge to FHA scenario. But the extent of downfall is not in same order; hence are not seemingly clear from the plot. Panel (c) suggests that, for ground state, **total PM Tsallis entropy** $T^{(\alpha,\beta)}$ grows with r_c and finally merges to FHA limit. But for all other states, $T^{(\alpha,\beta)}$'s slowly increase, then attain maxima and lastly falls off prior to joining with FHA. Positions of these maxima shift to right as n and number of nodes rise. Such attainment to FHA is not so conspicuous from panel (c), as they tend to approach much larger $(-)$ ve values with r_c . But upon closer examination, they follow same trend as exemplified by $2p$. Behavior of R_r^α and T_r^α with change of r_c are quite harmonious. But, variations of T_p^β and $T^{(\alpha,\beta)}$ with development of r_c are different from R_p^β and $R^{(\alpha,\beta)}$ patterns, even though, one can draw analogous conclusion from study of T and R . The graphs of T versus n (parallel to those in [Fig. 8](#) for R), offer resembling motives in their nature. Hence they are not separately presented here.

Now we move on to S in [Table X](#), where S_r, S_p and **total PM Shannon entropy** S are probed for lowest two $l = 0$ states of CHA at same particular set of r_c as in [Table VIII](#). **A handful of literature results are known for ground state; the reference values are duly quoted at r_c of 0.1, 0.2, 0.5, 0.6, 1, 3, 5, 10 and 40 a.u., whereas, for $2s$ state these have been considered only in the recent work of [35] at r_c values 0.2, 0.6, 1, 3, 5, 10, 20, 30 and 40 a.u.** Other than that we are not aware of any report on these quantities. Wherever applicable, present estimates are in decent agreement with reference data. S_r, S_p, S imprint exactly analogous behavior of R_r^α , R_p^β and $R^{(\alpha,\beta)}$ respectively. Like R_r^α , S_r 's also possess $(-)$ ve values for $1s$, $2s$ at very low r_c and then continuously evolve, until reaching FHA-limit at some large r_c . However, like R_p^β , S_p offers an opposite nature of $S_r(R_r^\alpha)$; from an initial $(+)$ ve, consistently diminishes to reach FHA, which for $2s$, assumes a $(-)$ ve (-0.75758) . One finds that, in smaller r_c region, $S_r(1s) > S_r(2s)$; but at close to r_c within 1-2, they cross each other. Likewise, in low to moderate r_c area, $S_p(1s) < S_p(2s)$; near the region of 7-7.5, $S_p(1s)$ overcomes $S_p(2s)$.

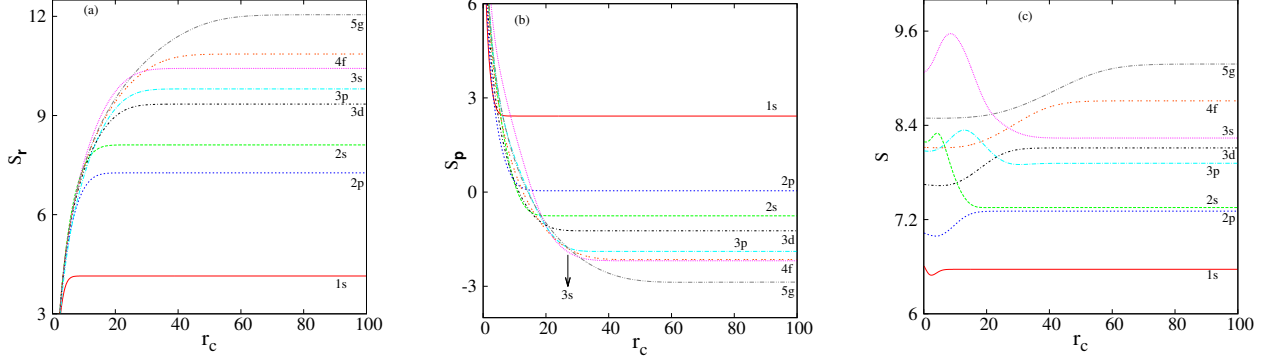


FIG. 9: Plot of S_r (a), S_p (b), **total PM Shannon entropy S** (c), in left, middle and right panels, against r_c for a few selected low-lying states of CHA. **S 's for all these states obey the lower bound condition given in Eq. (15).** More details are available in text.

Next, **Fig. 9** exhibits behavioral patterns of S_r , S_p , **total PM Shannon entropy S** with r_c in segments (a)-(c), for same eight states of Fig. 7. Note that, panels (a), (b), (c) of both **Figs. 7, 9** show similar style. For all of them, S_r 's mount up with r_c and finally converge to corresponding r -space FHA, while S_p 's deplete before attaining that. In case of S 's in panel (c), for node-less states ($1s, 2p, 3d, 4f, 5g$), one finds an initial decay until arriving at some minima and then an expansion again. As usual, FHA-limit is retrieved after some large r_c .

In **Fig. S2**, S_r (A), S_p (B), **total PM Shannon entropy S** (C) of $l = 0 - 4$ states are plotted against n at same six r_c of Fig. 8, in panels (a)-(f) from bottom to top. Again, the graphs in **Fig. S2** delineate similar shape and aptitude to that of Fig. 8. Thus, in agreement with R_r^α at $r_c = 0.1$, for five l , S_r 's get lowered in A(a), while S_p 's and S 's progress with n in B(a) and C(a) respectively. This augments our previous inference (as R in Fig. 8) that, at very low r_c , effect of confinement is more prevalent in high-lying states, signifying a magnification of quantum nature in such circumstances. As usual, like R_r^α and R_p^β here also, the first two columns (A, B) of **Fig. S2** render the appearance of a maximum and minimum in S_r ((b) upwards), S_p ((c) upwards) plots with successive growth of r_c . Their positions get shifted to right as r_c advances, which is indicative of the fact that, at $r_c \rightarrow \infty$ these plots merge to Figs. 5(a), 5(b) respectively (note that those graphs depicted radial quantities in r , p spaces). Column C suggests that at all r_c , S consistently broadens with n .

Now we discuss I in **Table XI**, by providing I_r , I_p of lowest two s states at selected r_c used in **Tables VIII, X**. As a check, I_r was calculated in two ways: first one using direct expression of **Eq. (14)** needing $\nabla\rho(\mathbf{r})$, and second one employing a simplified expression

TABLE XI: $I_{\mathbf{r}}, I_{\mathbf{p}}$ for $1s$ and $2s$ states in CHA at some particular r_c . See text for details.

$1s^\dagger$			$2s$		
r_c	$I_{\mathbf{r}}$	$I_{\mathbf{p}}$	r_c	$I_{\mathbf{r}}$	$I_{\mathbf{p}}$
0.1 ^a	3948.737092	0.01119745297	0.1	15791.82122	0.01284003608
0.2 ^b	987.8765878	0.04434444184	0.2	3948.29263	0.05141786856
0.3 ^c	439.586678	0.09875572074	0.3	1755.043513	0.11583040943
0.5 ^d	158.8961123	0.26851341481	0.5	632.0932498	0.32261837746
0.6	110.6681458	0.38237153819	0.6	439.0827084	0.46525991900
0.8	62.739860	0.66414501270	0.8	247.1624885	0.82981661465
1.0 ^e	40.58509174	1.01251135493	1.0	158.32289745	1.30128804642
1.5	18.79543801	2.12851618061	3.0	17.70794067	12.34353050970
2.5	7.90930147	4.99836645404	5.0	6.144128803	35.62201065982
3.0	6.17657298	6.49907451467	7.5	2.538369575	75.35119911871
4.0	4.67890854	9.08124532490	10.0	1.4882497628	114.09728048962
5.0 ^f	4.1962752	10.73988673564	12.0	1.1870576	138.20789171766
7.5	4.00555844	11.92721564499	15.0	1.037249102	158.95005505011
10.0	4.00009944	11.99783793184	20.0	1.001488032	167.39728283512
20.0	4.000000000	11.99999999999	30.0	1.0000006963	167.99942953967
40.0 ^g	4.000000000	12.00000000000	40.0	1.000000000	167.99999999101

^aReference result [37]: $I_{\mathbf{r}} = 3947.738178$, $I_{\mathbf{p}} = 0.011309$.

^bReference result [37]: $I_{\mathbf{r}} = 987.890146$, $I_{\mathbf{p}} = 0.043982$.

^cReference result [37]: $I_{\mathbf{r}} = 439.591750$, $I_{\mathbf{p}} = 0.099274$.

^dReference result [37]: $I_{\mathbf{r}} = 158.896729$, $I_{\mathbf{p}} = 0.269820$.

^eReference result [37]: $I_{\mathbf{r}} = 40.585607$, $I_{\mathbf{p}} = 1.012849$.

^fReference result [37]: $I_{\mathbf{r}} = 4.195911$, $I_{\mathbf{p}} = 10.740746$.

^gReference result [37]: $I_{\mathbf{r}} = 3.999875$, $I_{\mathbf{p}} = 11.999627$.

[†]Reference values are multiplied with a 4π factor

for central potentials requiring expectation values, namely Eq. (23). They produce almost identical results, which are quoted in table for two states. Note that gradient of density and integrands in expectation values for CHA can be evaluated analytically ($m = 0$ throughout). Only integrations needed to be performed numerically. Thus, it suffices to mention that, I 's can be accurately approached from a knowledge of $\langle p^2 \rangle$, $\langle r^{-2} \rangle$, $\langle r^2 \rangle$, $\langle p^{-2} \rangle$. Two possibilities may be envisaged: (i) first three evaluated in r , while $\langle p^{-2} \rangle$ in p space (ii) $\langle r^2 \rangle$, $\langle r^{-2} \rangle$ in r space, while $\langle p^2 \rangle$, $\langle p^{-2} \rangle$ in p space. Here we adopted route (i) which obviates the necessity to do numerical differentiation in either space (all integrands are available analytically). Once again literature reports are quite scanty; only for ground state some variational calculations were published in [37] for a few r_c . Present results show good agreement with these.

Now, Fig. 10 depicts the variation of $I_{\mathbf{r}}, I_{\mathbf{p}}$, total PM Fisher information $I = I_{\mathbf{r}}I_{\mathbf{p}}$, in three columns labeled (a)-(c) from left, with of r_c . Keeping same presentation strategy as in Fig. 7, these are offered for same eight states. The trends of I is completely opposite to

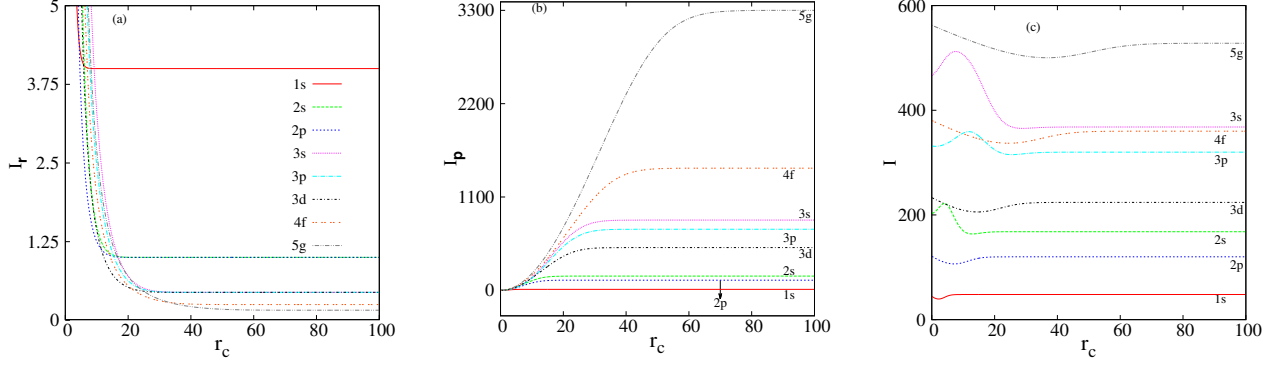


FIG. 10: Plot of I_r (a), I_p (b), **total PM Fisher information I** (c) in left, middle and right panels, against r_c for a few selected low-lying states of CHA. I 's for all these states obey the lower and upper bound conditions given in Eq. (14). More details can be found in text.

those observed in R , T , S . One notices from (a), (b) that, with r_c , I_r and I_p behave in an opposite fashion—former grows while latter falls. Eventually they both approach FHA values after a certain r_c . For node-less states in (c), I 's mount up and thereafter merge to FHA. But, for non-circular states, I 's rise towards certain maxima, ultimately falling flat at FHA.

Next, in Fig. S3, I_r , I_p , **total PM Fisher information I** are displayed for several $l=0-4$ states of CHA, as function of n at same six (corresponding to panels (a)-(f)) r_c of Fig. S2, in left (A), center (B), right (C) columns. At $r_c = 0.1$ in (a), I_r and I increase with n , while I_p behaves contrastingly. Thus, it follows that, at very low r_c , $\langle p^2 \rangle$ and n go hand in hand. This is exactly reverse to FHA case, as delineated before in Eq. (23), where the same shows inverse relationship with n . Once again, the quantum nature of high- n states intensifies at smaller r_c , possibly due to same reason as found in R , S . First two columns show that, a minimum and a maximum tends to develop as r_c progresses from lower to upper panels; their positions shift towards right on moving from (a) to (f). Here kinetic energy is gained with confinement and lost with addition of radial nodes. This establishes that, as r_c grows, effect of delocalization (number of nodes) predominates over localization, for lower n . Thus there appears minimum in I_r and maximum in I_p . Eventually at $r_c \rightarrow \infty$, first effect is switched off; hence $\langle p^2 \rangle$ as well as I_r lower with n and FHA situation is restored. In all r_c 's, I progress with n , in last column.

At this stage, we move on to the last measure in this study, i.e., E in Table XII. Here, the behavior compliments that of I before. A cross-section of E_r , E_p for $1s$, $2s$ states of CHA at same r_c values introduced previously in Table XI are offered. Once again we observe that,

TABLE XII: $E_{\mathbf{r}}, E_{\mathbf{p}}$ for $1s$ and $2s$ states in CHA at some chosen r_c . See text for details.

$1s$			$2s$		
r_c	$E_{\mathbf{r}}$	$E_{\mathbf{p}}$	r_c	$E_{\mathbf{r}}$	$E_{\mathbf{p}}$
0.1	685.2442626946369	0.000003957597	0.1	1467.6825381961700	0.0000005701644
0.2	87.4022739883438	0.000031421866	0.2	185.2798582651059	0.000004564133
0.3	26.4463446487399	0.00010521164	0.3	55.4384452351512	0.000015417924
0.5	5.9724213649058	0.0004788967	0.5	12.2085268184201	0.00007158083
0.6	3.5387151037986	0.0008200589	0.6	7.1325907889262	0.00012393792
0.8	1.5693288422636	0.0019064694	0.8	3.0655325000105	0.00029535230
1.0	0.8479175599159	0.0036453711	1.0	1.5979206523341	0.0005811807
1.5	0.2926831761804	0.011563379	3.0	0.0656052279197	0.02062639
2.5	0.0931826682370	0.045113309	5.0	0.0126465348027	0.17568481
3.0	0.0680640975474	0.069558611	7.5	0.0030330727129	1.0029980
4.0	0.0481916949634	0.123248904	10.0	0.0013566103366	2.6889282
5.0	0.0421759263287	0.167061238	12.0	0.0009842621480	4.3151579
7.5	0.0398551249937	0.20591605	15.0	0.0008167874743	6.30370206
10.0	0.0397899027431	0.208864145	20.0	0.0007786672679	7.5080031
20.0	0.0397887357477	0.208974941	30.0	0.0007771237450	7.6497493
40.0	0.0397887357477	0.208974941	40.0	0.0007771237450	7.6497493

at small r_c , $E_{\mathbf{r}}(1s) < E_{\mathbf{r}}(2s)$, which reverses after around $r_c \approx 3$. On the other hand, at moderately large (around 5) r_c , $E_{\mathbf{p}}(2s)$ exceeds $E_{\mathbf{p}}(1s)$. None of these have been reported before; hence cannot be compared.

Above changes of $E_{\mathbf{r}}, E_{\mathbf{p}}$, **total PM Onicescu energy E** with r_c are graphically displayed in Fig. 11, in left (a), middle (b), right (c) panels, for eight low-lying states. Like $I_{\mathbf{r}}$ in Fig. 10, $E_{\mathbf{r}}$ falls off with r_c , with ground state remaining well separated from others; all finally converging to FHA. Similarly, $E_{\mathbf{p}}$, like $I_{\mathbf{p}}$ of Fig. 10 again, rises with r_c ; then merges to FHA. At last, they converge to E of FHA. In Fig. (S4), $E_{\mathbf{r}}, E_{\mathbf{p}}$ and **total PM Onicescu energy E** are depicted (in columns A, B, C) for $l=0-4$ states as function of n at six different r_c (in segments (a)-(f)). At the lowest r_c considered, these three behave qualitatively quite similarly as the respective I 's in Fig. 13; $E_{\mathbf{r}}$ climb up while $E_{\mathbf{p}}, E$ record an opposite trend with n . This is in accordance with our earlier finding that, at very low r_c , confinement is more on higher states. First two columns suggest that, a minimum and maximum appears in $E_{\mathbf{r}}, E_{\mathbf{p}}$ graphs as r_c gets extended. As in Fig. (S3), positions of these extrema also shift towards right upon proceeding from bottom to top panels in columns A, B. This supports that, at $r_c \rightarrow \infty$ CHA gets modified to FHA. Lastly the rightmost column records variation of **total PM Onicescu energy E** against n . In all r_c 's, E tend to grow with n .

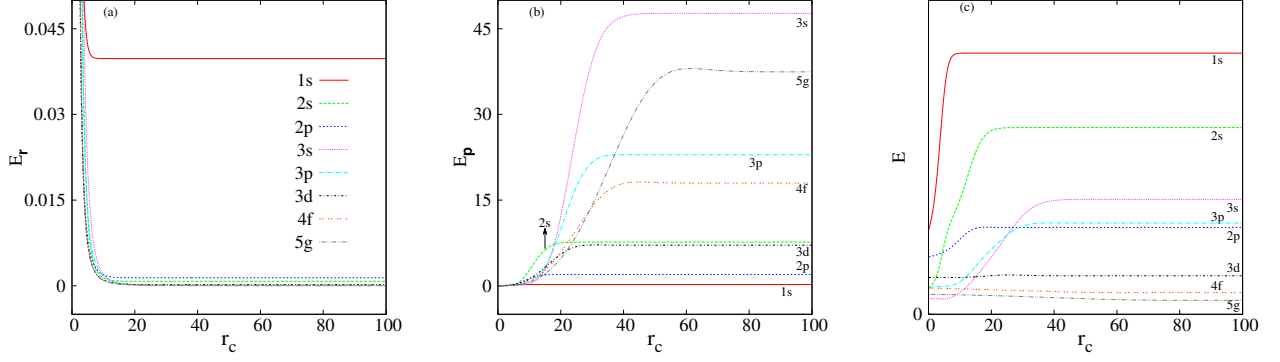


FIG. 11: Variation of E_r , E_p and E with r_c for CHA. For more details, see text.

IV. FUTURE AND OUTLOOK

Information theoretic measures like R , T , S , I , E are pursued for a FHA and CHA in both r , p spaces, along with their **total PM measures**. Accurate results of angular contributions to R , T , S , E are reported for $l \leq 9$ states ($m = 0$), besides their radial counterparts. For CHA, *combined* or total information measures (radial *plus* angular) are provided.

In FHA, for *node-less states*, while *exact* analytical expressions for I , S have been published, the same for R , T , E are as yet unknown and derived here, again in both r , p space. Illustrative calculations were made for both s and non-zero l states ($1s - 4f$, $10s - 10m$), out of which R , T and E are completely new. It is found that, with growth of n , R_r , T_r , S_r increase and E_r decreases, which effectively points to the addition of radial node as well as spread of wave function. Thus, these quantities may be exploited to understand the diffuse nature of orbitals, especially for high-lying states. Like FHA, R , T , E for all states are given first time in a CHA. For S , I , even, excepting the lowest state, all results are new here. Among many interesting features, one notices that, at very low r_c , kinetic energy rises, while R_r^α , T_r^β , S_r fall, as n advances, which is in sharp contrast to that found in FHA.

Overall, we have presented an elaborate account of the nature of a multitude of information measures under hard confinement. Further, it establishes the validity and utility of R , T , S , I , E in the context of confinement in a CHA. These may be useful to explore the so-called *complexity* measures in a CHA, in future. There are several open questions that may lead to important conclusions and requires further scrutiny, such as, the effect of non-zero m and a penetrable cavity. It may also be worthwhile to examine these quantities in the realm of Rydberg states under certain boundary conditions. A parallel inspection on many-electron systems would be highly desirable.

V. ACKNOWLEDGEMENT

Financial support from DST SERB, New Delhi, India (sanction order: EMR/2014/000838) is gratefully acknowledged. NM thanks DST SERB, New Delhi, India, for a National-post-doctoral fellowship (sanction order: PDF/2016/000014/CS). Critical constructive comments from two anonymous referees is greatly appreciated.

- [1] A. Michels, J. de Boer and A. Bijl, *Physica* **4**, 981 (1937).
- [2] J. R. Sabin, E. Brändas and S. A. Cruz (Eds.), *The Theory of Confined Quantum Systems*, Parts I and II, *Advances in Quantum Chemistry*, Vols. 57 and 58 (Academic Press, 2009).
- [3] K. D. Sen (Ed.), *Electronic Structure of Quantum Confined Atoms and Molecules*, (Springer, Switzerland, 2014).
- [4] A. Sarsa and C. Le Sech, *J. Chem. Theory Comput.* **7**, 2786 (2011).
- [5] C. Le Sech and A. Banerjee, *J. Phys. B* **44**, 105003 (2011).
- [6] J. Katriel and H. E. Montgomery Jr., *J. Chem. Phys.* **137**, 114109 (2012).
- [7] R. Cabrera-Trujillo and S. A. Cruz, *Phys. Rev. A* **87**, 012502 (2013).
- [8] H. Pang, W-S. Dai and M. Xie, *J. Phys. A* **44**, 365001 (2011).
- [9] N. Aquino, *J. Phys. A* **30**, 2403 (1997).
- [10] G. Campoy, N. Aquino and V. D. granados, *J. Phys. A* **35**, 4903 (2002).
- [11] H. E. Montgomery Jr., N. A. Aquino and K. D. Sen, *Int. J. Quant. Chem.* **107**, 798, (2007)
- [12] A. K. Roy, *Mod. Phys. Lett. A* **29**, 1450104 (2014); *ibid.*, **30**, 1550176 (2015).
- [13] A. Ghosal, N. Mukherjee and A. K. Roy, *Ann. Phys. (Berlin)* **528**, 796, (2016).
- [14] S. Goldman and C. Joslin, *J. Phys. Chem.* **96**, 6021 (1992).
- [15] N. Aquino A., *Int. J. Quant. Chem.* **54**, 107 (1995).
- [16] J. Garza, R. Vargas and A. Vela, *Phys. Rev. E* **58**, 3949 (1998).
- [17] C. Laughlin, B. L. Burrows and M. Cohen, *J. Phys. B* **35**, 701 (2002).
- [18] B. L. Burrows and M. Cohen, *Int. J. Quant. Chem.* **106**, 478 (2006).
- [19] N. Aquino, G. Campoy and H. E. Montgomery Jr., *Int. J. Quant. Chem.* **107**, 1548 (2007).
- [20] D. Baye and K. D. Sen, *Phys. Rev. E* **78**, 026701 (2008).
- [21] H. Ciftci, R. L. Hall and N. Saad, *Int. J. Quant. Chem.* **109**, 931 (2009).

- [22] A. K. Roy, *Int. J. Quant. Chem.* **115**, 937 (2015).
- [23] K. D. Sen (Ed.), *Statistical Complexity: Applications in Electronic Structure*, (Springer, 2012).
- [24] E. Romera, P. Sánchez-Moreno and J. S. Dehesa, *Chem. Phys. Lett.* **414**, 468 (2005).
- [25] E. Romera, P. Sánchez-Moreno and J. S. Dehesa, *J. Math. Phys.* **47**, 103504 (2006).
- [26] J. S. Dehesa, S. López-Rosa, B. Olmos and R. J. Yáñez, *J. Math. Phys.* **47**, 052104 (2006).
- [27] J. S. Dehesa, R. González-Férez and P. Sánchez-Moreno, *J. Phys. A* **40**, 1845 (2007).
- [28] P. Sánchez-Moreno, S. Zozor and J. S. Dehesa, *J. Math. Phys.* **52**, 022105 (2011).
- [29] I. V. Toranzo, D. Puertas-Centeno and J. S. Dehesa, *Physica A* **462**, 1197 (2016).
- [30] R. J. Yáñez, W. Van Assche and J. S. Dehesa, *Phys. Rev. A* **50**, 3065 (1994).
- [31] I. V. Toranzo and J. S. Dehesa, *Euro Phys. Lett.* **113**, 48003 (2016).
- [32] J. Katriel and K. D. Sen, *J. Comput. Appl. Math.* **233**, 1399 (2010).
- [33] J. S. Dehesa, S. López-Rosa, A. Martínez-Finkelshtein and R. J. Yáñez, *Int. J. Quant. Chem.* **110**, 1529 (2010).
- [34] K. D. Sen, *J. Chem. Phys.* **123**, 074110 (2005).
- [35] L. G. Jiao, L. R. Zan, Y. Z. Zhang and Y. K. Ho, *Int. J. Quant. Chem.* **117**, e25375 (2017).
- [36] S. H. Patil, K. D. Sen, N. A. Watson and H. E. Montgomery Jr., *J. Phys. B* **40**, 2147 (2007).
- [37] N. Aquino, A. Flores-Riveros and J. F. Rivas-Silva, *Phys. Lett. A* **377**, 2062 (2013).
- [38] G.-H. Sun, M. A. Aoki and S.-H. Dong, *Chin. Phys. B* **22**, 050302 (2013).
- [39] G.-H. Sun, S.-H. Dong and N. Saad, *Ann. Phys. (Berlin)* **525**, 934 (2013).
- [40] W. A. Yahya, K. J. Oyewumi and K. D. Sen, *Int. J. Quant. Chem.* **115**, 1543 (2015).
- [41] S. Dong, G.-H. Sun, S.-H. Dong and J. P. Draayer, *Phys. Lett. A* **378**, 124 (2014).
- [42] R. Valencia-Torres, G.-H. Sun and S.-H. Dong, *Phys. Scr.* **90**, 035205 (2015).
- [43] G.-H. Sun, P. Duan, C.-N. Oscar and S.-H. Dong, *Chin. Phys. B* **24**, 100303 (2015).
- [44] G. Yáñez-Navarro, G.-H. Sun, T. Dytrych, K. D. Launey, S.-H. Dong and J. P. Draayer, *Ann. Phys.* **348**, 153 (2014).
- [45] X.-D. Song, G.-H. Sun and S.-H. Dong, *Phys. Lett. A* **379**, 1402 (2015).
- [46] G.-H. Sun, S.-H. Dong, K. D. Launey, T. Dytrych and J. P. Draayer, *Int. J. Quant. Chem.* **115**, 891 (2015).
- [47] S. Liu, *J. Chem. Phys.* **126**, 191107 (2007).
- [48] Á. Nagy, *Chem. Phys. Lett.* **449**, 212 (2007).
- [49] J. B. Szabó, K. D. Sen and Á. Nagy, *Phys. Lett. A* **372**, 2428 (2008).

- [50] O. Onicescu, C. R. Acad. Sci. Paris A **263**, 25 (1966).
- [51] N. Mukherjee, A. Roy and A. K. Roy, Ann. Phys. (Berlin) **527**, 825, (2015).
- [52] N. Mukherjee and A. K. Roy, Ann. Phys. (Berlin) **528**, 412, (2016).
- [53] R. G. González-Férez and J. S. Dehesa, Phys. Rev. Lett. **91**, 113001 (2003).
- [54] I. Bialynicki-Birula, Phys. Rev. A **74**, 052101 (2006).
- [55] I. Bialynicki-Birula and J. Mycielski, Commun. Math. Phys. **44**, 129, (1975).
- [56] I. Varga and J. Pipek, Phys. Rev. E **68**, 026202 (2003).
- [57] R. Renner, N. Gisin and B. Kraus, Phys. Rev. A **72**, 012332 (2005).
- [58] P. Lévy, S. Negy and J. Pipek, Phys. Rev. A **72**, 022302 (2005).
- [59] F. Verstraete and J. I. Cirac, Phys. Rev. B **73**, 094423 (2006).
- [60] A. Bialas, W. Czyz and K. Zalewski, Phys. Rev. C **73**, 034912 (2006).
- [61] L. L. Salcedo, J. Math. Phys. **50**, 012106 (2009).
- [62] S.-B. Liu, C.-Y. Rong, Z.-M. Wu and T. Lu, Acta. Phys.-Chim. Sin. **31**, 2057 (2015).
- [63] M. Gell-Mann and C. Tsallis (Eds.), *Nonextensive Entropy-Interdisciplinary Applications*, Chapter I, (Oxford University Press, 2004).
- [64] J. Naudts, *Generalised Thermostatistics*, Springer, London, 2011.
- [65] A. R. Plastino and A. Plastino, Braz. J. Phys. **29**, 79 (1999).
- [66] J. Chen and G. Li, Entropy **16**, 3009 (2014).
- [67] A. K. Roy, J. Phys. G **30**, 269 (2004).
- [68] K. D. Sen and A. K. Roy, Phys. Lett. A **357**, 112 (2006).
- [69] A. K. Roy, Int. J. Quant. Chem. **113**, 1503 (2013); *ibid.*, **114**, 383 (2014).
- [70] J. Sañudo and R. López-Ruiz, Phys. Lett. A **372**, 5283 (2008).
- [71] C. Tsallis, J. Stat. Phys. **52** 479 (1988).